AERO-ASTRONAUTICS REPORT NO. 246

GAMMA GUIDANCE OF TRAJECTORIES FOR COPLANAR, AEROASSISTED ORBITAL TRANSFER

by

A. MIELE AND T. WANG

RICE UNIVERSITY

1990

AERO-ASTRONAUTICS REPORT NO. 246

GAMMA GUIDANCE OF TRAJECTORIES FOR COPLANAR, AEROASSISTED ORBITAL TRANSFER

by

A. MIELE AND T. WANG

RICE UNIVERSITY

1990

Gamma Guidance of Trajectories for Coplanar, Aeroassisted Orbital Transfer[1]

by

A. Miele[2] and T. Wang[3]

[1]This research was supported by NASA Marshall Space Flight Center Grant No. NAG-8-820, by Jet Propulsion Laboratory Contract No. 956415, and by Texas Advanced Technology Program Grant No. TATP-003604020.

[2]Foyt Family Professor of Aerospace Sciences and Mathematical Sciences, Aero-Astronautics Group, Rice University, Houston, Texas.

[3]Senior Research Scientist, Aero-Astronautics Group, Rice University, Houston, Texas.

Abstract. This paper is concerned with the optimization and guidance of trajectories for coplanar, aeroassisted orbital transfer (AOT) from high Earth orbit (HEO) to low Earth orbit (LEO). In particular, HEO can be a geosynchronous Earth orbit (GEO). It is assumed that the initial and final orbits are circular, that the gravitational field is central and is governed by the inverse square law, and that at most three impulses are employed, one at HEO exit, one at atmospheric exit, and one at LEO entry. It is also assumed that, during the atmospheric pass, the trajectory is controlled via the lift coefficient. The presence of upper and lower bounds on the lift coefficient is considered.

First, optimal trajectories are computed by minimizing the total velocity impulse (hence, the propellant consumption) required for AOT transfer. Use is made of the sequential gradient-restoration algorithm (SGRA) for optimal control problems. It is shown that the optimal trajectory includes two branches: a relatively short descending flight branch (branch 1) and a long ascending flight branch (branch 2).

In branch 1, the path inclination ranges from a few degrees negative to zero and is nearly a linear function of the altitude; in branch 2, the path inclination ranges from zero to a fraction of a degree positive and is a slowly varying function of the altitude. Velocity depletion takes place along the entire atmospheric trajectory, but is concentrated mostly in the terminal part of branch 1 and the beginning part of branch 2. As

the ratio of HEO radius to LEO radius increases, the minimum altitude of the optimal trajectory decreases, implying that a deeper penetration into the atmosphere is required.

Next, attention is focused on guidance trajectories capable of approximating the optimal trajectories in real time, while retaining the essential characteristics of simplicity, ease of implementation, and reliability. For the atmospheric pass, a feedback control scheme is employed and the lift coefficient is adjusted according to a two-stage gamma guidance law. For branch 1, the gamma guidance is a linear path inclination guidance; for branch 2, the gamma guidance is a constant path inclination guidance. The switch from branch 1 guidance to branch 2 guidance is governed by the requirement that a specified apogee be reached, following the atmospheric exit. Computer simulations show that, by proper selection of four guidance parameters (the entry path inclination γ_0, the target altitude h_T of branch 1, the switch velocity V_S, and the target path inclination γ_T of branch 2), the gamma guidance trajectory can be made close to the optimal trajectory.

Further improvements are possible via a modified gamma guidance, which differs from the gamma guidance as follows: in the gamma guidance, the parameters V_S, γ_T are preselected; in the modified gamma guidance, V_S, γ_T are adjusted in flight with a predictor-corrector algorithm; also, the target altitude of the modified gamma guidance is lower than that of the gamma guidance. Computer simulations show that the modified gamma guidance trajectory is superior to the gamma guidance trajectory in the following sense:

it is more stable with respect to dispersion effects arising from navigation errors, variations of the atmospheric density, and uncertainties in the aerodynamic coefficients.

A byproduct of the studies on dispersion effects is the following design concept. For coplanar aeroassisted orbital transfer, the lift-range-to-weight ratio appears to play a more important role than the lift-to-drag ratio. This is because the lift-range-to-weight ratio controls mainly the minimum altitude (hence, the peak heating rate) of the guidance trajectory; on the other hand, the lift-to-drag ratio controls mainly the duration of the atmospheric pass of the guidance trajectory.

Key Words. Optimization, guidance, gamma guidance, modified gamma guidance, parameter dispersion effects, flight mechanics, astrodynamics, aeroassisted orbital transfer, sequential gradient-restoration algorithm.

1. Introduction

Saving propellant weight and increasing the payload are among the most important problems of space transportation. Orbital transfer from high Earth orbit (HEO) to low Earth orbit (LEO) can be made more economic if the aeroassisted orbital transfer (AOT) mode is employed. In the AOT mode, use is made of the aerodynamic forces in order to achieve the proper amount of velocity depletion during the atmospheric pass. Here, the intent is to achieve a specified apogee following the atmospheric exit, while minimizing the overall propellant consumption and keeping the peak heating rate within reasonable bounds during the atmospheric pass.

Aeroassisted orbital transfer is not only important for HEO-to-LEO transfer maneuvers, but may prove to be indispensable for future planetary flights. In particular, this statement refers to lunar return vehicles, Mars exploration vehicles, and Mars return vehicles.

Over the past several years, considerable research has been done on two aspects of coplanar, aeroassisted orbital transfer: trajectory optimization (Refs. 1-7) and trajectory guidance (Refs. 8-12). Concerning trajectory guidance for lift-modulated AOT, see the work of Mease and McCreary (Ref. 9), Lee and Grantham (Ref. 10), and Miele, Wang, and Lee (Ref. 12). In particular, in Ref. 12, a two-stage guidance scheme, consisting of the combination of target altitude guidance and target path inclination

guidance, was developed for the atmospheric pass of an AOT spacecraft, akin to the target altitude guidance already developed for the abort landing of an aircraft in a windshear (Ref. 13).

This paper continues the work of Ref. 12 and develops a two-stage gamma guidance for the atmospheric pass of an AOT spacecraft, akin to the gamma guidance already developed for the abort landing of an aircraft in a windshear (Ref. 14). Indeed, there are similarities between these two situations: (i) both trajectories are characterized by descending flight, followed by near-horizontal flight, followed by ascending flight; (ii) both trajectories are characterized by energy dissipation; (iii) both trajectories are dangerous unless proper guidance and control are applied. However, there are also differences between these two situations: (i) the performance index of the AOT spacecraft is the characteristic velocity, while the performance index of the abort landing aircraft is the altitude drop; (ii) the energy dissipation of the AOT spacecraft is due to the aerodynamic forces, while the energy dissipation of the abort landing aircraft is due to the combination of shear and downdraft; (iii) reaching a specified apogee after the atmospheric pass is essential for the AOT spacecraft, while reaching a specified altitude after the windshear encounter is not essential for the abort landing aircraft. The similarities suggest that the gamma guidance scheme developed for abort landing in a windshear can be adapted in concept to the atmospheric pass of an AOT spacecraft.

The differences suggest that major modifications are necessary.

With the above ideas in mind, this paper is organized as follows. Section 2 contains the notations, and Section 3 presents the system description. In Section 4, we study optimal trajectories, namely, trajectories minimizing the propellant consumption required for orbital transfer. We observe that, during the atmospheric pass, the optimal trajectory includes a relatively short descending flight branch (branch 1) and a long ascending flight branch (branch 2). We also observe that the path inclination of the optimal trajectory can be approximated by a linear function of the altitude in branch 1 and by a constant value in branch 2.

For the guidance trajectory, this leads to a two-stage gamma guidance (Section 5), in which the guidance law is a linear path inclination guidance in branch 1 and a constant path inclination guidance in branch 2. Next, via computer simulations, we select the four guidance parameters of the gamma guidance, namely, the entry path inclination γ_0, the target altitude h_T of branch 1, the switch velocity V_S, and the target path inclination γ_T of branch 2. Having developed the gamma guidance, we then proceed to developing the modified gamma guidance (Section 6), in which the parameters γ_0, h_T are preselected, while the parameters V_S, γ_T are adjusted in flight via a predictor-corrector algorithm; in addition, the target altitude of the modified gamma guidance is lower than that of the gamma guidance. Finally, we test the modified gamma guidance with respect to dispersion

effects arising from navigation errors, variations of the atmospheric density, and uncertainties in the aerodynamic coefficients (Section 7). The conclusions are given in Section 8.

2. Notations

Throughout this paper, the following notations are employed:

C_D = drag coefficient;

C_{DO} = zero-lift drag coefficient;

C_L = lift coefficient;

D = drag, N;

g = local acceleration of gravity, m/sec^2;

h = altitude, m;

H = $r_a - r_e$ = thickness of the atmosphere, m;

HR = heating rate, W/m^2;

K = induced drag factor;

K = gain coefficient;

L = lift, N;

m = mass, kg;

r = radial distance from the center of the Earth, m;

r_e = radius of the Earth, m;

r_a = radius of the outer edge of the atmosphere, m;

S = reference surface area, m^2;

t = T/τ = dimensionless time;

T = running time, sec;

V = velocity, m/sec;

V_a = $\sqrt{(\mu/r_a)}$ = circular velocity at $r = r_a$, m/sec;

γ = path inclination, rad;

μ = Earth's gravitational constant, m^3/sec^2;

ρ = air density, kg/m^3;

τ = final time, sec;

ΔV = characteristic velocity, m/sec.

Subscripts

'0 = entry into the atmosphere;

1 = exit from the atmosphere;

00 = exit from the initial orbit;

11 = entry into the final orbit.

Superscripts

. = derivative with respect to dimensionless time;

~ = condition following the application of a velocity impulse or nominal condition.

3. System Description

In this section, we consider coplanar, aeroassisted orbital transfer from high Earth orbit to low Earth orbit. We employ the following assumptions: (i) the initial and final orbits are circular; (ii) three impulses are employed, one at the exit from the initial orbit, one at the exit from the atmosphere, and one at the entry into the final orbit; and (iii) the gravitational field is central and is governed by the inverse square law. The four key points of the maneuver are these: point 00, exit from the initial orbit; point 0, entry into the atmosphere; point 1, exit from the atmosphere; and point 11, entry into the final orbit; see Fig. 1.

The maneuver starts in high Earth orbit with a tangential propulsive burn, having characteristic velocity ΔV_{00}, at point 00; here, the spacecraft enters into an elliptical transfer orbit, connecting the points 00 and 0; this elliptical transfer orbit is such that its apogee occurs at r_{00}. At point 0, the spacecraft enters into the atmosphere; after traversing the upper layers of the atmosphere, it exits from the atmosphere at point 1; during the atmospheric pass, the velocity of the spacecraft is depleted, due to the aerodynamic drag. At point 1, the maneuver continues with a tangential propulsive burn, having characteristic velocity ΔV_1; then, the spacecraft enters into an elliptical transfer orbit connecting the points 1 and 11; this elliptical transfer orbit is such that its apogee occurs at r_{11}. The maneuver ends with a

tangential propulsive burn, having characteristic velocity ΔV_{11}, at point 11; here, the spacecraft enters into the low Earth orbit, in that the magnitude of ΔV_{11} is such that the desired circularization into LEO is achieved.

3.1. Atmospheric Pass. For the atmospheric portion of the trajectory of the AOT vehicle, we employ the following hypotheses: (i) the atmospheric pass is made with engine shut-off; hence, in this portion of the flight, the AOT vehicle behaves as a particle of constant mass; (ii) Coriolis acceleration terms and transport acceleration terms are neglected; (iii) the spacecraft is controlled via the lift coefficient; (iv) the aerodynamic forces are evaluated using the inertial velocity, rather than the relative velocity; (v) under extreme hypersonic conditions, the dependence of the aerodynamic coefficients on the Mach number and the Reynolds number is disregarded.

3.2. Differential System. With the above assumptions, and upon normalizing the flight time to unity, the equations of motion are given by

$$\dot{h} = \tau[V\sin\gamma], \tag{1a}$$

$$\dot{V} = \tau[-D/m - g\sin\gamma], \tag{1b}$$

$$\dot{\gamma} = \tau[L/mV + (V/r - g/V)\cos\gamma], \tag{1c}$$

with $0 \leq t \leq 1$. In the above equations,

$$r = r_e + h, \qquad g = \mu/r^2 = \mu/(r_e + h)^2, \tag{2}$$

where μ denotes the Earth's gravitational constant. In addition, the aerodynamic forces are given by

$$D = (1/2)C_D\rho SV^2, \qquad L = (1/2)C_L\rho SV^2, \tag{3a}$$

with $\rho = \rho(h)$. In particular, if a parabolic polar is postulated, the relation between the drag coefficient and the lift coefficient is given by

$$C_D = C_{D0} + KC_L^2. \tag{3b}$$

3.3. Control Constraint. To obtain realistic solutions, the presence of upper and lower bounds on the lift coefficient is necessary. Therefore, the two-sided inequality constraint

$$C_{La} \leq C_L \leq C_{Lb} \tag{4}$$

must be satisfied everywhere along the interval of integration.

3.4. Boundary Conditions. At the entry into the atmosphere ($t = 0$) and at the exit from the atmosphere ($t = 1$), certain static and dynamic boundary conditions must be satisfied. Specifically, at atmospheric entry, we have

$$h_0 = H, \tag{5a}$$

$$r_{00}^2(2V_a^2 - V_0^2) - 2r_{00}r_aV_a^2 + r_a^2V_0^2\cos^2\gamma_0 = 0, \tag{5b}$$

where H is the thickness of atmosphere and V_a is the circular velocity at $r = r_a$. In addition, at atmospheric exit, we have

$$h_1 = H, \tag{6a}$$

$$r_{11}^2(2V_a^2 - \tilde{V}_1^2) - 2r_{11}r_aV_a^2 + r_a^2\tilde{V}_1^2\cos^2\gamma_1 = 0. \tag{6b}$$

Note the following: (i) the entry condition (5a) implies that $r_0 = r_a$; (ii) the entry condition (5b) arises from energy conservation and angular momentum conservation applied to the HEO-to-entry transfer orbit; (iii) the exit condition (6a) implies that $r_1 = r_a$; (iv) the exit condition (6b) arises from energy conservation and angular momentum conservation applied to the exit-to-LEO transfer orbit; (v) because the velocity impulse ΔV_1 is applied at atmospheric exit, the following relation holds:

$$\Delta V_1 = \tilde{V}_1 - V_1; \tag{7a}$$

here, V_1 and $\tilde{V}_1$ denote the values of the exit velocity before and after the application of the propellant burn; (vi) in the light of the exit condition (6b), the value of the exit velocity after the application of the propellant burn can be written as

$$\tilde{V}_1 = V_a\sqrt{[2(r_{11}^2 - r_{11}r_a)/(r_{11}^2 - r_a^2\cos^2\gamma_1)]}. \tag{7b}$$

3.5. Summary. The relations governing the atmospheric pass include: the differential system (1)-(3), the control constraint (4), and the boundary conditions (5)-(6). In this formulation, the independent variable is the time t, $0 \leq t \leq 1$. The dependent variables include the state variables h(t), V(t), $\gamma(t)$, the control variable $C_L(t)$, and the parameter τ.

3.6. Experimental Data. The following data are used in the numerical experiments for optimal trajectories and guidance trajectories (Sections 4-7).

Spacecraft. For the spacecraft, it is assumed that the mass per unit reference surface area is $m/S = 300$ kg/m^2; the zero-lift drag coefficient is $C_{D0} = 0.1$; the induced drag factor is $K = 1.11$; the lift coefficient for maximum lift-to-drag ratio is $C_{LE} = 0.3$; the maximum lift-to-drag ratio is $E_{max} = 1.5$; the bounds on the lift coefficient are $C_{La} = -0.9$ and $C_{Lb} = +0.9$.

Physical Constants. The major physical constants used in the computations are as follows: the radius of the Earth is $r_e = 6378$ km; the radius of the outer edge of the atmosphere is $r_a = 6498$ km; the thickness of the atmosphere is $H = 120$ km; and the Earth's gravitational constant is $\mu = 0.3986E+06$ km^3/sec^2.

Transfer Maneuvers. Three transfer maneuvers are considered, involving different values of the HEO radius, but the same value of the LEO radius. To describe these maneuvers, let α and β denote the dimensionless ratios

$$\alpha = r_{00}/r_a, \qquad \beta = r_{11}/r_a. \tag{8}$$

Case 1. The HEO1 radius is $r_{00} = 12996$ km, $\alpha = 2$. The LEO radius is $r_{11} = 6558$ km, $\beta = 1.00923$.

Case 2. The HEO2 radius is $r_{00} = 25992$ km, $\alpha = 4$. The LEO radius is $r_{11} = 6558$ km, $\beta = 1.00923$.

Case 3. The HEO3 radius is $r_{00} = 42164$ km, $\alpha = 6.48877$.

The LEO radius is r_{11} = 6558 km, β = 1.00923. Note that HEO3 = GEO.

Atmospheric Model. The atmospheric model used is the US Standard Atmosphere, 1976 (Ref. 15). In this model, the values of the density are tabulated at discrete altitudes. For intermediate altitudes, the density is computed by assuming an exponential fit for the function $\rho(h)$. This is equivalent to assuming that the atmosphere behaves isothermally between any two contiguous altitudes tabulated in Ref. 15.

Heating Rate. The heating rate HR is computed with the relation

$$HR = C\sqrt{(\rho/\rho_R)}\,(V/V_R)^{3.08}. \qquad (9)$$

Here, ρ_R = 0.39957E-02 kg/m^3 is a reference density (density at the reference altitude h_R = 40 km) and $V_R = V_a$ = 7.832 km/sec is a reference velocity. The constant C represents the heating rate at $V = V_R$ and $h = h_R$; its value is assumed to be C = 348.7 W/cm^2.

4. Optimal Trajectories

4.1. Performance Index. Subject to the previous constraints, different AOT optimization problems can be formulated, depending on the performance index chosen. The resulting optimal control problems are either of the Bolza type or of the Chebyshev type. In this paper, only one performance index is considered, the minimum energy required for orbital transfer.A measure of this energy is the total characteristic velocity ΔV, the sum of the characteristic velocity ΔV_{00} associated with the propulsive burn from the initial orbit, the characteristic velocity ΔV_1 associated with the propulsive burn at the exit of the atmosphere, and the characteristic velocity ΔV_{11} associated with the propulsive burn into the final orbit. Clearly,

$$I = \Delta V = \Delta V_{00} + \Delta V_1 + \Delta V_{11}, \tag{10a}$$

with

$$\Delta V_{00} = \sqrt{(r_a/r_{00})}V_a - (r_a/r_{00})V_0\cos\gamma_0, \tag{10b}$$

$$\Delta V_1 = \tilde{V}_1 - V_1, \tag{10c}$$

$$\Delta V_{11} = \sqrt{(r_a/r_{11})}V_a - (r_a/r_{11})\tilde{V}_1\cos\gamma_1. \tag{10d}$$

In the last two equations, $\tilde{V}_1$ is supplied by Eq. (7b).

4.2. Numerical Results. Optimal trajectories were computed by minimizing the performance index (10), subject to the constraining relations. Three transfer maneuvers were considered: HEO1-to-LEO, HEO2-to-LEO, and HEO3-to-LEO; see Cases 1,2,3 of Section 3. The

sequential gradient-restoration algorithm was employed in primal form (Refs. 16-18). This is a first-order algorithm which generates a sequence of feasible solutions, each characterized by a lower value of the performance index (10). The numerical results are shown in Tables 1-2 and Fig. 2.

Table 1 presents the following quantities: the entry values of the altitude, the velocity, and the path inclination; the exit values of the altitude, the velocity, and the path inclination; the minimum altitude, the peak heating rate, and the flight time; the characteristic velocity components and the total characteristic velocity.

Table 2 compares the values of the total characteristic velocity for three trajectories: the optimal AOT trajectory, computed accounting for the control constraint (4); the ideal optimal AOT trajectory, computed disregarding the control constraint (4); this is the so-called grazing trajectory; and the optimal space trajectory; this is the so-called Hohmann transfer trajectory.

Figure 2 contains four parts: the altitude h versus the time t (Fig. 2A); the velocity V versus the time t (Fig. 2B); the path inclination γ versus the time t (Fig. 2C); and the lift coefficient C_L versus the time t (Fig. 2D).

From Tables 1-2 and Fig. 2, the following comments arise:

(i) The optimal trajectory includes two branches: a relatively short descending flight branch (branch 1) and a long

ascending flight branch (branch 2). As the HEO radius increases, the minimum altitude of the optimal trajectory decreases, implying that a deeper penetration into the atmosphere is required to ensure the proper amount of velocity depletion.

(ii) Velocity depletion takes place along the entire atmospheric trajectory, but is concentrated mostly in the terminal part of branch 1 and the beginning part of branch 2.

(iii) The path inclination increases rapidly from the entry value (a few degrees negative) to zero value in branch 1; and it increases slowly from zero value to the exit value (a fraction of a degree positive) in branch 2.

(iv) The lift coefficient profile is nearly independent of the HEO radius. In branch 1, the lift coefficient decreases rapidly from the upper bound value to nearly the lower bound value; in branch 2, the lift coefficient stays near the lower bound value.

(v) For all the transfer cases studied, the characteristic velocity of the optimal trajectory is close to that of the ideal grazing trajectory. The excess expenditure in ΔV characterizing the optimal trajectory vis-a-vis the ideal grazing trajectory is 1.5% for Case 1, is 0.9% for Case 2, and is 0.6% for Case 3 (GEO-to-LEO transfer).

(vi) As the HEO radius increases, the advantage of the optimal trajectory vis-a-vis the Hohmann trajectory increases. The relative saving in ΔV is 52.2% in Case 1, is 57.8% in Case 2, and is 61.5% in Case 3.

4.3. Guidance Implications. Consider the altitude-path inclination domain and, with reference to Fig. 2, regard the altitude profile $h = h(t)$ and the path inclination profile $\gamma = \gamma(t)$ as parametric representation of the trajectory, the time t being the parameter. Upon elimination of the time, one obtains the path inclination-altitude relation $\gamma = \gamma(h)$. Then, this relation can be rewritten in the normalized form $\theta = \theta(\eta)$, where θ and η denote normalized variables defined as follows:

$$\theta = \gamma/|\gamma_0|, \quad \text{branch 1,} \tag{11a}$$

$$\theta = \gamma/|\gamma_0|, \quad \text{branch 2,} \tag{11b}$$

and

$$\eta = (h_0 - h)/(h_0 - h_{min}), \quad \text{branch 1,} \tag{12a}$$

$$\eta = (h - h_{min})/(h_0 - h_{min}), \quad \text{branch 2.} \tag{12b}$$

The normalized path inclination-altitude relation $\theta = \theta(\eta)$ is plotted in Fig. 3, which contains two parts: the descending flight branch (Fig. 3A) and the ascending flight branch (Fig. 3B). For branch 1, the normalized path inclination is nearly a linear function of the normalized altitude, and its slope is relatively steep; for branch 2, the normalized path inclination is also nearly a linear function of the normalized altitude, but its slope is relatively shallow. These observations are the basis of the gamma guidance law described in Section 5. This is a two-stage guidance law, designed as follows: for branch 1, the gamma

guidance is a linear path inclination guidance; for branch 2, the gamma guidance is a constant path inclination guidance.

5. Gamma Guidance Trajectories

In the previous sections, optimal trajectories for coplanar AOT flight were determined. They include three phases: the preatmospheric phase, characterized by the velocity impulse ΔV_{00} at HEO and the fact that the apogee of the HEO-to-entry transfer orbit occurs at r_{00}; the atmospheric phase, characterized by properties (i)-(vi) of Section 4; and the postatmospheric phase, characterized by the fact that $\Delta V_1 = 0$ at atmospheric exit, by the velocity impulse ΔV_{11} at LEO, and by the fact that the apogee of the exit-to-LEO transfer orbit occurs at r_{11}.

In this section, we develop gamma guidance trajectories for coplanar AOT flight under two basic requirements: (a) the gamma guidance trajectory (GGT) should be close to the optimal trajectory (OT); and (b) the gamma guidance trajectory should be simple, easy to implement, and reliable.

For the preatmospheric phase and the postatmospheric phase, we control the guidance trajectory via the velocity impulses ΔV_{00} and ΔV_{11}, albeit with slightly different values from those of the optimal trajectory, in order to increase reliability. In addition, at atmospheric exit, we introduce into the guidance trajectory the velocity impulse ΔV_1 in order to compensate for previous velocity errors and ensure that the specified apogee can be reached.

For the more complicated atmospheric phase, we structure the guidance trajectory so as to reproduce the two-branch geometry of the optimal trajectory: a relatively short descending

flight branch (branch 1); and a long ascending flight branch (branch 2). To achieve the above properties, we employ a feedback control scheme, and we adjust the lift coefficient according to a two-stage gamma guidance law. For branch 1, the gamma guidance is a linear path inclination guidance; for branch 2, the gamma guidance is a constant path inclination guidance. We investigate the proper selection of four guidance parameters, namely: the initial path inclination γ_0; the target altitude h_T of branch 1; the switch velocity V_S from branch 1 to branch 2; and the target path inclination γ_T of branch 2.

5.1. Preatmospheric Phase. Initially, the spacecraft is in a high Earth orbit of radius r_{00}. To deorbit, the following velocity impulse is applied:

$$\Delta V_{00} = \sqrt{(r_a/r_{00})}V_a - (r_a/r_{00})V_0\cos\gamma_0, \tag{13a}$$

with

$$V_0 = V_a\sqrt{[2(r_{00}^2 - r_{00}r_a)/(r_{00}^2 - r_a^2\cos^2\gamma_0)]}. \tag{13b}$$

This enables the spacecraft to enter into an elliptical transfer orbit leading from HEO exit to atmospheric entry. In Eqs.(13), r_{00} is the HEO radius, r_a is the radius of the outer edge of the atmosphere, and V_a is the circular velocity at $r = r_a$. Because r_a, V_a are constant and r_{00} is given, Eqs. (13) imply that $V_0 = V_0(\gamma_0)$ and $\Delta V_{00} = \Delta V_{00}(\gamma_0)$. Hence, the selection of the entry angle γ_0 determines uniquely both the entry velocity V_0 and the initial velocity impulse ΔV_{00}.

5.2. Atmospheric Phase. The atmospheric phase includes the descending flight branch (branch 1) and the ascending flight branch (branch 2). For both branches, a gamma guidance scheme is implemented in feedback control form. The switch from branch 1 to branch 2 is regulated by the switch velocity V_S, to be selected appropriately.

Descending Flight Branch. For branch 1, the gamma guidance is a linear path inclination guidance, which is implemented in the following feedback control form:

$$C_L - \tilde{C}_L(h,V,\gamma) = -K_1(\gamma - \tilde{\gamma}), \tag{14a}$$

$$\tilde{\gamma} = \gamma_0(h - h_T)/(h_0 - h_T), \tag{14b}$$

$$C_{La} \leq C_L \leq C_{Lb}. \tag{14c}$$

Here, C_L is the instantaneous lift coefficient and $\tilde{C}_L$ is the nominal lift coefficient; C_{La} and C_{Lb} are the lower and upper bounds for the lift coefficient; γ is the instantaneous path inclination, $\tilde{\gamma}$ is the nominal path inclination, and γ_0 is the entry path inclination; h is the instantaneous altitude, h_0 is the entry altitude, and h_T is the target altitude; and K_1 is the gain coefficient for path inclination error. With reference to (14), the following remarks are pertinent.

(a) The nominal lift coefficient $\tilde{C}_L$ is computed with Eq. (1c) under the assumption of near-equilibrium conditions. Upon setting $\dot{\gamma} \cong 0$, invoking Eqs. (2)-(3), and observing that $\rho = \rho(h)$, $r = r(h)$, and $g = g(h)$, we obtain the relation

$$(1/2)C_L\rho(h)SV^2 + m[V^2/r(h) - g(h)]\cos\gamma = 0, \tag{15a}$$

which admits the solution

$$\tilde{C}_L = 2m[g(h) - V^2/r(h)]\cos\gamma/\rho(h)SV^2, \tag{15b}$$

which has the form

$$\tilde{C}_L = \tilde{C}_L(h,V,\gamma). \tag{15c}$$

(b) The target altitude h_T should be in a proper range. If h_T is too high, the guidance trajectory is flat, resulting in an early exit from the atmosphere;because not enough velocity is depleted in the atmospheric pass, this results in large values of the characteristic velocity. If h_T is too low, the guidance trajectory is too steep, resulting in deeper penetration of the atmosphere; therefore, the peak heating rate is too high.

In practice, the target altitude should be selected so as to be below, but close to, the minimum altitude of the OT. One option is to prescribe directly h_T; another option is to prescribe indirectly h_T, based on the selection of the target lift coefficient C_{LT}. The second option is preferable, because this procedure compensates automatically for variations of the atmospheric density with respect to the standard density.

Next, observe that $\gamma = 0$ at the target altitude. Then, with reference to Eq. (15b), replace $\tilde{C}_L$, h, V with C_{LT}, h_T, V_T,

where the subscript T denotes target value. This yields the relation

$$C_{LT} = 2m[g(h_T) - V_T^2/r(h_T)]/\rho(h_T)SV_T^2, \tag{16a}$$

where

$$V_T = 0.25V_0 + 0.75V_1. \tag{16b}$$

Here, V_0 is the entry velocity of the OT and V_1 is the exit velocity of the OT. Because V_0, V_1 are known, V_T is known. Hence, Eqs. (16) yield the one-to-one relation

$$C_{LT} = C_{LT}(h_T), \tag{17a}$$

whose inverse form is

$$h_T = h_T(C_{LT}). \tag{17b}$$

Therefore, prescribing the target lift coefficient C_{LT} is equivalent to prescribing the target altitude h_T. At any rate, the choice of C_{LT} should be consistent with Ineq. (4); in addition, there should be enough margin on both the lower bound side and the upper bound side for control.

(c) The gain coefficient for path inclination error is given by

$$K_1 = \rho_*/\rho, \tag{18}$$

where $\rho = \rho(h)$ is the air density at the altitude h and $\rho_* = \rho(h_*)$ is the air density at the reference altitude $h_* = H/3 = 40$ km.

This particular form of the gain coefficient is justified by the need for a more energetic control response at higher altitudes and a gentler control response at lower altitudes.

(d) Finally, it must be observed that the feedback form (14) of the gamma guidance has two important properties: (a) it is strongly stable at the target altitude; this is because $\tilde{\gamma} < 0$ if $h > h_T$, while $\tilde{\gamma} > 0$ if $h < h_T$; and (b) it avoids overshooting and undershooting of the target altitude, since $\tilde{\gamma}$ varies smoothly between the entry value $\tilde{\gamma} = \gamma_0$ and the target altitude value $\tilde{\gamma} = 0$.

Ascending Flight Branch. For branch 2, the gamma guidance is a constant path inclination guidance, which is implemented via the following feedback control form:

$$C_L - \tilde{C}_L(h,V,\gamma) = -K_2(\gamma - \tilde{\gamma}), \tag{19a}$$

$$\tilde{\gamma} = \gamma_T, \tag{19b}$$

$$C_{La} \leq C_L \leq C_{Lb}. \tag{19c}$$

Here, γ_T denotes the target path inclination and K_2 is the gain coefficient for path inclination error. With reference to (19), the following comments are pertinent.

(a) The target path inclination γ_T should be in a proper range. If γ_T is too small, the exit from the atmosphere might become physically impossible. If γ_T is too large, the characteristic velocity component ΔV_{11} might become too large. Finally, the selection of γ_T should be consistent with the selection of the switch velocity V_S, so as to ensure that the

desired apogee can be reached after the atmospheric pass.

(b) The gain coefficient for path inclination error is given by

$$K_2 = \rho_*/\rho, \tag{20}$$

where $\rho = \rho(h)$ is the air density at the altitude h and $\rho_* = \rho(h_*)$ is the air density at the reference altitude $h_* = H/3 = 40$ km. Once more, this particular form of the gain coefficient is justified by the need for a more energetic control response at higher altitudes and a gentler control response at lower altitudes.

5.3. Postatmospheric Phase. The postatmospheric phase includes two velocity impulses: a velocity impulse ΔV_1 at atmospheric exit and a velocity impulse ΔV_{11} at LEO entry.

Atmospheric Exit. The velocity impulse at atmospheric exit is determined with the relation

$$\Delta V_1 = \tilde{V}_1 - V_1, \tag{21a}$$

where

$$\tilde{V}_1 = V_a\sqrt{[2(r_{11}^2 - r_{11}r_a)/(r_{11}^2 - r_a^2\cos^2\gamma_1)]}. \tag{21b}$$

This velocity impulse is essential for the GGT in order to compensate for previous velocity errors. In Eqs. (21), r_{11} is the LEO radius, r_a is the radius of the outer edge of the atmosphere, V_a is the circular velocity at $r = r_a$, γ_1 is the exit path inclination, V_1 is the exit velocity prior to the velocity impulse, and $\tilde{V}_1$ is the exit velocity after the application of the velocity

impulse. Note that r_a, V_a are constant, r_{11} is given, and V_1, γ_1 are measured in actual flight.

LEO Entry. After the velocity impulse (21) is applied, the spacecraft enters into an elliptical transfer orbit leading from atmospheric exit to LEO entry. This elliptical transfer orbit is such that its apogee occurs at r_{11}. At this point, the velocity impulse ΔV_{11} is applied so as to achieve circularization into LEO. Specifically, ΔV_{11} is determined with the relation

$$\Delta V_{11} = \sqrt{(r_a/r_{11})}V_a - V_{11}. \tag{22a}$$

In Eq. (22a), r_a is the radius of the outer edge of the atmosphere, V_a is the circular velocity at $r = r_a$, r_{11} is the LEO radius, and V_{11} is the velocity at LEO entry prior to the velocity impulse. Note that r_a, V_a are constant, r_{11} is given, and V_{11} is measured in actual flight. However, in the computer simulations, the measurement of V_{11} is replaced by the relation

$$V_{11} = (r_a/r_{11})\tilde{V}_1\cos\gamma_1, \tag{22b}$$

which arises from angular momentum conservation applied to the exit-to-LEO transfer orbit. In Eq. (22b), $\tilde{V}_1$ is supplied by Eq. (21b).

5.4. Guidance Parameters. As explained in the previous sections, the behavior of the guidance scheme described by Eqs. (13)-(22) depends on four parameters: the entry path inclination γ_0; the target altitude h_T; the switch velocity V_S; and the target path inclination γ_T.

(a) The entry path inclination γ_0 should be in a proper range. If $|\gamma_0|$ is too small, the guidance trajectory is too flat, resulting in an early exit from the atmosphere; because not enough velocity is depleted in the atmospheric pass, this results in large values of the characteristic velocity. If $|\gamma_0|$ is too large, the guidance trajectory is too steep, resulting in deeper penetration of the atmosphere; therefore, the peak heating rate is too high.

Good results are obtained by choosing $|\gamma_0|$ of the GGT to be somewhat larger than $|\gamma_0|$ of the OT. Note that the entry path inclination γ_0 determines automatically the entry velocity V_0 and the HEO propulsive impulse ΔV_{00}; see Eqs. (13).

(b) The target altitude h_T should not be too high nor too low. If h_T is too high, the guidance trajectory is flat, resulting in an early exit from the atmosphere; because not enough velocity is depleted in the atmospheric pass, this results in large values of the characteristic velocity. If h_T is too low, the guidance trajectory is too steep, resulting in deeper penetration of the atmosphere; therefore, the peak heating rate is too high.

Good results are obtained by choosing h_T of the GGT to be somewhat lower than h_{min} of the OT. As explained in Section 5.2, this goal is achieved indirectly by prescribing the target lift coefficient C_{LT} corresponding to near-equilibrium level flight.

(c) The switch velocity V_S should also be in a proper range. The best choice of V_S should be such that the exit velocity of

the GGT is close to the exit velocity of the OT. If this is done, the velocity impulse at atmospheric exit ΔV_1 is small.

In practice, the switch velocity V_S of the GGT is chosen to be a weighted average of the entry velocity V_0 of the OT and the exit velocity V_1 of the OT,

$$V_S = V_1 + A(V_0 - V_1), \tag{23a}$$

where the dimensionless constant A is to be selected appropriately. Equation (23a) means that the switch velocity V_S is compatible with the target altitude h_T. Indeed, the higher the entry velocity V_0, the lower the minimum altitude h_{min} of the OT, hence the lower the target altitude h_T of the GT; to guarantee the same value of the exit velocity V_1, a higher switch velocity V_S is needed for the GT, which is the case with Eq.(23a).

(d) The target path inclination γ_T should be in a proper range. If γ_T is too small, the exit from the atmosphere might become physically impossible. If γ_T is too large, the characteristic velocity component ΔV_{11} might become too large.

In practice, the target path inclination γ_T of the GGT is chosen to be some fraction of the exit path inclination γ_1 of the OT,

$$\gamma_T = B\gamma_1, \tag{23b}$$

where the dimensionless constant B is to be selected appropriately.

5.5. Numerical Results. To investigate the effect of the four guidance parameters γ_0, h_T, V_S, γ_T on the GGT, a large number of combinations were tried, and the corresponding guidance trajectories were computed. Typical combinations of guidance parameters are shown in Table 3 for Case 1, Case 2, and Case 3. These combinations were selected because the resulting GGT is geometrically close to the corresponding OT, so as to retain the good features of the OT concerning the total characteristic velocity

$$\Delta V = \Delta V_{00} + \Delta V_1 + \Delta V_{11} \tag{24}$$

and the peak heating rate.

More detailed information about the GGT is shown in Table 4. This table presents the following quantities: the entry values of the altitude, the velocity, and the path inclination; the exit values of the altitude, the velocity,and the path inclination; the minimum altitude, the peak heating rate, and the flight time; the characteristic velocity components and the total characteristic velocity.

Table 5 compares the GGT and the OT from the point of view of the total characteristic velocity ΔV.

Tables 6-8 present a more detailed comparison of the GGT and the OT from the point of view of these quantities: the entry values of the altitude, the velocity,and the path inclination; the exit values of the altitude, the velocity, and the path inclination; the minimum altitude, the peak heating rate, and

the flight time; the characteristic velocity components and the total characteristic velocity.

Finally, Figs. 4-6 present a graphical comparison of the GGT and the OT in terms of the altitude profile h(t), the velocity profile V(t), the path inclination profile $\gamma(t)$, and the lift coefficient profile $C_L(t)$.

From Tables 3-8 and Figs. 4-6, the following comments arise.

(i) The altitude profile of the GGT is close to the altitude profile of the OT and retains the two-branch geometry of the OT: a relatively short descending flight branch (branch 1); and a long ascending flight branch (branch 2). As the HEO radius increases, the minimum altitude of the GGT decreases, consistently with the behavior of the OT.

(ii) The velocity profile of the GGT is close to the velocity profile of the OT. Velocity depletion takes place along the entire atmospheric trajectory, but is concentrated mostly in the terminal part of branch 1 and the beginning part of branch 2.

(iii) The path inclination profile of the GGT is close to the path inclination profile of the OT. In branch 1, the path inclination increases almost linearly from the entry value to zero value; in branch 2, the path inclination increases slowly from zero value to the exit value.

(iv) The lift coefficient profile of the GGT is close to the lift coefficient profile of the OT. In branch 1, the lift coefficient decreases rapidly from the upper bound value to the lower bound value; in branch 2, the lift coefficient stays near the lower bound value.

(v) The characteristic velocity of the GGT is quite close to the characteristic velocity of the OT. The relative increase in ΔV is 1.3% for Case 1, 0.7% for Case 2, and 0.1% for Case 3. This small increase is almost exclusively due to the fact that $\Delta V_1 \neq 0$ for the GGT, while $\Delta V_1 = 0$ for the OT. In other words, while the OT exits from the atmosphere with the correct values of V_1 and γ_1, this is not the case with the GGT. Hence, at atmospheric exit, a nonzero, albeit small, velocity impulse is needed for the GGT.

(vi) The peak heating rate (PHR) of the GGT is somewhat higher than the peak heating rate of the OT. The relative increase in PHR is 9.4% for Case 1, 4.7% for Case 2, and 7.7% for Case 3. The higher peak heating rate of the GGT vis-a-vis the OT is due to the larger value of $|\gamma_0|$ and the corresponding lower target altitude, which in turn cause a deeper penetration into the atmosphere. This increase in $|\gamma_0|$ and the corresponding decrease in h_T cannot be avoided, because of the need for stability of the gamma guidance trajectory.

6. Modified Gamma Guidance Trajectories

In real AOT flights, there are dispersion effects arising from navigation errors, variations of the atmospheric density, and uncertainties in the aerodynamic coefficients. Navigation errors refer to the space portion of AOT flights and induce errors in the entry path inclination; density variations are due to such factors as latitude, season, time of the day or the night, solar activity or are due to lack of sufficient knowledge of a particular planetary atmosphere (Mars); uncertainties in the aerodynamic coefficients arise because wind tunnel tests might not simulate precisely the combination of high speeds and low densities characterizing AOT flights or arise because CFD schemes[4] might not account precisely for all of the physical factors involved.

While the gamma guidance scheme of Section 5 yields a trajectory close to the optimal trajectory in the absence of parameter dispersion effects, this scheme is not sufficiently robust with respect to large parameter dispersion. For the sake of discussion, let unprimed quantities denote standard values; let primed quantities denote dispersed values; and let the following dispersion factors be defined:

$$F_{\gamma 0} = \gamma_0'/\gamma_0, \tag{25a}$$

$$F_{\rho} = \rho'(h)/\rho(h), \tag{25b}$$

[4] CFD is an acronym for computational fluid dynamics.

$$F_{CD0} = C'_{D0}/C_{D0}, \tag{25c}$$

$$F_K = K'/K, \tag{25d}$$

$$F_{CLR} = (C'_{Lb} - C'_{La}) /(C_{Lb} - C_{La}). \tag{25e}$$

Here, F_{γ_0} is the entry path inclination factor; F_ρ is the density factor; F_{CD0} is the zero-lift drag factor; F_K is the induced drag factor; and F_{CLR} is the lift range factor. If there are no dispersion effects,

$$F_{\gamma_0} = 1, \quad F_\rho = 1, \quad F_{CD0} = 1, \quad F_K = 1, \quad F_{CLR} = 1. \tag{26}$$

However, if there are dispersion effects, one or more of the above factors might be different from unity.

As an example, consider the entry path inclination factor (25a) in connection with Case 3; if $F_{\gamma_0} = 0.93$, corresponding to $\Delta\gamma_0 = +0.3$, the GGT skips out of the atmosphere with little velocity dissipation; in turn, this results in a large value of the characteristic velocity. As another example, consider the density factor (25b), and assume that its value is constant, independent of the altitude; if $F_\rho = 1/3$, the GGT skips out of the atmosphere. As a third example, consider the induced drag factor (25d); if $F_\rho = 1/2$, the GGT skips out of the atmosphere; if $F_\rho = 2$, the GGT penetrates too deeply into the atmosphere, ultimately leading to a crash.

There are two ways for improving the stability of the gamma guidance scheme with respect to dispersion effects:

(i) to lower the target altitude; (ii) to adjust the switch velocity and the target path inclination by means of a predictor-corrector algorithm. The resulting trajectory is called modified gamma guidance trajectory (MGGT).

6.1. Target Altitude and Entry Path Inclination. From the point of view of the total characteristic velocity and the peak heating rate, the target altitude should be as high as possible; hence, it should be as close as possible to the minimum altitude of the optimal trajectory. While the GGT of Section 5 achieves this goal, it is marginally stable with respect to dispersion effects.

With the MGGT, the goal is to increase the stability with respect to dispersion effects, while keeping the total characteristic velocity and the peak heating rate within reasonable range. The increased stability is achieved by lowering the target altitude h_T, hence increasing the target lift coefficient C_{LT}. To achieve compatibility between the target altitude and the entry path inclination γ_0, steeper values of the entry path inclination might be desirable.

6.2. Switch Velocity and Target Path Inclination. Because of parameter dispersion effects, the ideal condition $\Delta V_1 = 0$ cannot be achieved. However, ΔV_1 can be kept small by adjusting the switch velocity and the target path inclination in such a way that ΔV_1 is less than some threshold value, for instance, $\Delta V_1 \leq 0.03$ km/sec. This can be achieved via the predictor-corrector algorithm described below.

6.3. Predictor-Corrector Algorithm. This algorithm includes five steps. The description of these steps is given below with particular reference to Case 3, GEO-to-LEO transfer.

Step 1. Assume that the spacecraft is at the end of branch 1 with switch altitude and switch path inclination given by

$$h_S = h_T, \quad \gamma_S = 0. \tag{27}$$

Assume that the switch velocity is

$$V_S = V_1 + A(V_0 - V_1) \tag{28a}$$

and that the target path inclination of branch 2 is

$$\gamma_T = B\gamma_1. \tag{28b}$$

Here, V_0 is the entry velocity of the optimal trajectory; V_1 is the exit velocity of the optimal trajectory; γ_1 is the exit path inclination of the optimal trajectory; and A, B are dimensionless constants to be specified appropriately.

The predictor-corrector algorithm starts by assuming that

$$V_S = 8.40 \text{ km/sec}, \quad \gamma_T = 0.15 \text{ deg}, \tag{29a}$$

corresponding to

$$A \cong 0.25, \quad B \cong 0.50. \tag{29b}$$

Step 2. For branch 2, integrate Eqs. (1)-(3) in forward time using the feedback control form (19) of the constant path inclination guidance. Determine the exit values V_1, γ_1 of the guidance trajectory.

Step 3. Verify whether the inequality

$$\Delta V_1 \leq 0.03 \quad \text{km/sec} \tag{30}$$

is satisfied. If this is the case, accept the assumed pair (A,B), hence the assumed pair (V_S, γ_T); the predicted-corrector procedure is terminated. Otherwise, go to either Step 4 (if V_1 must be increased) or Step 5 (if V_1 must be decreased).

Step 4. This step must be performed if compliance with Ineq. (30) requires that V_1 be increased. It consists of two successive one-dimensional searches, first in the A-direction, while keeping B = const (Step 4A), and then in the B-direction, while keeping A = const (Step 4B).

Step 4A. For B = const, hence γ_T = const, subject the parameter A to increments ΔA corresponding to increments ΔV_S = 0.10 km/sec. For each value of A, hence for each value of V_S, execute Step 2. The search in the A-direction stops if Ineq. (30) is satisfied simultaneously with V_S < 9.10 km/sec; in such a case, the assumed (A,B) pair is accepted, and the predictor-corrector procedure is terminated. However, if the value V_S = 9.10 km/sec is reached without satisfaction of Ineq. (30), then go to Step 4B.

Step 4B. For A = const, corresponding to V_S = 9.10 km/sec, subject the parameter B to increments ΔB corresponding to increments $\Delta\gamma_T$ = 0.01 deg. For each value of B, hence for each value of γ_T, execute Step 2. The search in the B-direction stops if Ineq. (30) is satisfied; in such a case, the assumed (A,B)

pair is accepted, and the predictor-corrector procedure is terminated.

Step 5. This step must be performed if compliance with Ineq. (30) requires that V_1 be decreased. It consists of a single one-dimensional search in the A-direction, while keeping B = const.

For B = const, hence γ_T = const, subject the parameter A to decrements ΔA corresponding to decrements ΔV_S = -0.05 km/sec. For each value of A, hence for each value of V_S, execute Step 2. The search in the A-direction stops if Ineq. (30) is satisfied; in such a case, the assumed (A,B) pair is accepted, and the predictor-corrector procedure is terminated.

6.4. Numerical Results. Here, we present a comparative study of the GGT and the MGGT for Case 3, GEO-to-LEO transfer. This study is done in the absence of dispersion effects, that is, under assumptions (26). Dispersion effects are analyzed systematically in Section 7.

For both the GGT and the MGGT, Table 9 presents typical combinations of the guidance parameters.

For both the GGT and the MGGT, Table 10 shows the following quantities: the entry values of the altitude, the velocity and the path inclination; the exit values of the altitude, the velocity, and the path inclination; the minimum altitude, the peak heating rate, and the flight time; the characteristic velocity components and the total characteristic velocity.

Finally, Fig. 7 presents a graphical comparison of the GGT and the MGGT in terms of the altitude profile h(t), the velocity

profile V(t), the path inclination profile $\gamma(t)$, and the lift coefficient profile $C_L(t)$.

From Tables 9-10 and Fig. 7, following comments arise.

(i) The altitude profile of the MGGT lies below the altitude profile of the GGT.

(ii) The velocity profile of the MGGT is relatively close to the velocity profile of the GGT.

(iii) The path inclination profile of the MGGT is relatively close to the path inclination profile of the GGT.

(iv) The lift coefficient profile of the MGGT is quite different from the lift coefficient profile of the GGT in that an ampler lift coefficient margin now exists with respect to the lower bound value.

(v) The characteristic velocity of the MGGT is quite close to the characteristic velocity of the GGT. The relative increase in ΔV is 0.4%.

(vi) The peak heating rate of the MGGT is somewhat higher than the peak heating rate of the GGT. The relative increase is 23.9%.The higher peak heating rate of the MGGT is due to deeper penetration into the atmosphere (by 3.1 km), which in turn is tied to the larger value of $|\gamma_0|$ and the lower value of h_T. This increase in $|\gamma_o|$ and decrease in h_T constitute the price which must be paid for the increased stability of the modified gamma guidance trajectory.

7. Parameter Dispersion Effects

As pointed out in Section 6, parameter dispersion effects are important in real AOT flights; therefore, they must be considered in the evaluation of the merits of a particular guidance scheme. In this section, we consider the modified gamma guidance scheme of Section 6 and explore the behavior of the MGGT vis-a-vis deviations from unity of the dispersion factors (25).

With reference to Case 3, GEO-to-LEO transfer, the results are shown in Tables 11-15 and Fig. 8. They demonstrate that the MGGT is capable of executing safely the atmospheric pass in the following range of values of the dispersion factors:

$$0.91 \leq F_{\gamma 0} \leq 1.44, \tag{31a}$$

$$0.33 \leq F_{\rho} \leq 10.00, \tag{31b}$$

$$0.10 \leq F_{CD0} \leq 5.00, \tag{31c}$$

$$0.10 \leq F_{K} \leq 5.00, \tag{31d}$$

$$0.33 \leq F_{CLR} \leq 3.00. \tag{31e}$$

A detailed discussion follows.

7.1. Entry Path Inclination Factor. See Table 11 and Fig. 8A. The MGGT is stable for values of the entry path inclination factor in the range

$$0.91 \leq F_{\gamma 0} \leq 1.44, \tag{32a}$$

corresponding to

$$-4.1 \geq \gamma_0 \geq -6.5 \text{ deg}, \tag{32b}$$

$$+0.4 \geq \Delta\gamma_0 \geq -2.0 \text{ deg}. \tag{32c}$$

In the above range, the target altitude, the switch velocity, and the target path inclination are constant. It must be noted that, if $F_{\gamma 0} = 0.89$, corresponding to $\gamma_0 = -4.0$ deg and $\Delta\gamma_0 = +0.5$ deg, the MGGT skips out of the atmosphere. On the other hand, if $F_{\gamma 0} = 1.44$, corresponding to $\gamma_0 = -6.5$ deg and $\Delta\gamma_0 = -2.0$ deg, the MGGT undershoots the target altitude. This situation is due to the fact that only a simple proportional feedback control is used in this paper and can be alleviated by employing more sophisticated forms of feedback control.

7.2. Density Factor. See Table 12 and Fig. 8B. The MGGT is stable for values of the density factor in the range

$$0.33 \leq F_\rho \leq 10.00. \tag{33}$$

In the above range, the entry path inclination, the switch velocity, and the target path inclination are constant. Both the target altitude and the peak heating rate increase as F_ρ increases. It is clear from (33) that the modified gamma guidance can tolerate large density increases better than large density decreases. In particular, if $F_\rho = 0.25$, the MGGT skips out of the atmosphere with a large increase in characteristic velocity.

7.3. Zero-Lift Drag Factor. See Table 13 and Fig. 8C. The MGGT is stable for values of the zero-lift drag factor in the range

$$0.10 \leq F_{CD0} \leq 5.00. \tag{34}$$

In the above range, the entry path inclination and the target altitude are constant. As F_{CD0} increases, the switch velocity increases, while the flight time decreases considerably. The increase in switch velocity is due to the fact that, as F_{CD0} increases, more energy is depleted for ascending from the target altitude to the atmospheric exit altitude. It is clear from (34) that the modified gamma guidance is able to tolerate both large increases and large decreases in zero-lift drag.

7.4. Induced Drag Factor. See Table 14 and Fig. 8D. The MGGT is stable for values of the induced drag factor in the range

$$0.10 \leq F_K \leq 5.00. \tag{35}$$

In the above range, the entry path inclination and the target altitude are constant. As F_K increases, the switch velocity increases, while the flight time decreases considerably. The increase in switch velocity is due to the fact that,as F_K increases, more energy is depleted for ascending from the target altitude to the atmospheric exit altitude.

It is clear from (35) that the modified gamma guidance is able to tolerate both large increases and large decreases in induced drag.

7.5. Lift Range Factor. See Table 15 and Fig. 8E. The MGGT is stable for values of the lift range factor such that

$$0.33 \leq F_{CLR} \leq 3.00. \tag{36}$$

In the above range, the entry path inclination and the target path inclination are constant. As F_{CLR} increases, the target altitude increases, the switch velocity decreases, and the target lift coefficient, which is negative, becomes larger in modulus; indeed, C_{LT} is proportional to F_{CLR}. As F_{CLR} increases, the peak heating rate decreases considerably, and the flight time changes somewhat. Generally speaking, the MGGT is more able to tolerate large increases in F_{CLR} than large decreases. In particular, if $F_{CLR} = 0.25$, the MGGT skips out of the atmosphere with a large increase in characteristic velocity.

8. Conclusions

This paper is concerned with the optimization and guidance of trajectories for coplanar, aeroassisted orbital transfer from high Earth orbit to low Earth orbit. The following major conclusions are obtained:

(i) The optimal trajectories include two branches: a relatively short descending flight branch (branch 1) and a long ascending flight branch (branch 2). In branch 1, the path inclination ranges from a few degrees negative to zero and is nearly a linear function of the altitude; in branch 2, the path inclination ranges from zero to a fraction of a degree positive and is a slowly varying function of the altitude.

(ii) Gamma guidance trajectories are developed so as to approximate the optimal trajectories in real time, while retaining the essential characteristics of simplicity, ease of implementation, and reliability. For the atmospheric pass, a feedback control scheme is employed and the lift coefficient is adjusted according to a two-stage gamma guidance law. For branch 1, the gamma guidance is a linear path inclination guidance; for branch 2, the gamma guidance is a constant path inclination guidance. By proper selection of four guidance parameters (the entry path inclination, the target altitude of branch 1, the switch velocity, and the target path inclination of branch 2), the gamma guidance trajectory can be made close to the optimal trajectory.

(iii) Improvements in stability are possible via a modified gamma guidance, which differs from the gamma guidance in that the switch velocity and the target path inclination are adjusted in flight with a predictor-corrector algorithm; also, the target altitude is lower and the entry path inclination is steeper. Computer simulations show that the modified gamma guidance trajectory is quite stable with respect to dispersion effects arising from navigation errors, variations of the atmospheric density, and uncertainties in the aerodynamic coefficients.

(iv) A byproduct of the parameter dispersion studies is the following design concept. For coplanar, aeroassisted orbital transfer, the lift-range-to-weight ratio appears to play a more important role than the lift-to-drag ratio. This is because the lift-range-to-weight ratio controls mainly the minimum altitude (hence, the peak heating rate) of the guidance trajectory; on the other hand, the lift-to-drag ratio controls mainly the duration of the atmospheric pass of the guidance trajectory.

References

1. MEASE, K. D., and VINH, N. X., Minimum-Fuel Aeroassisted Coplanar Orbit Transfer Using Lift Modulation, Journal of Guidance, Control, and Dynamics, Vol. 8, No. 1, pp. 134-141, 1985.

2. MIELE, A., and VENKATARAMAN, P., Optimal Trajectories for Aeroassisted Orbital Transfer, Acta Astronautica, Vol. 11, Nos. 7-8, pp. 423-433, 1984.

3. MIELE, A., and BASAPUR, V. K., Approximate Solutions to Minimax Optimal Control Problems for Aeroassisted Orbital Transfer, Acta Astronautica, Vol. 12, No. 10, pp. 809-818, 1985.

4. MIELE, A., BASAPUR, V. K., and MEASE, K. D., Nearly-Grazing Optimal Trajectories for Aeroassisted Orbital Transfer, Journal of the Astronautical Sciences, Vol. 34, No. 1, pp. 3-18, 1986.

5. MIELE, A., BASAPUR, V. K., and LEE, W. Y., Optimal Trajectories for Aeroassisted, Coplanar Orbital Transfer, Journal of Optimization Theory and Applications, Vol. 52, No. 1, pp. 1-24, 1987.

6. MEASE, K. D., Optimization of Aeroassisted Orbital Transfer: Current Status, Journal of the Astronautical Sciences, Vol. 36, Nos. 1-2, pp. 7-33, 1988.

7. MIELE, A., WANG, T., LEE, W. Y., and ZHAO, Z. G., Optimal Trajectories for the Aeroassisted Flight Experiment, Paper No. IAF-89-361, 40th Congress of the International Astronautical Federation, Malaga, Spain, 1989.

8. VINH, N. X., JOHANNESEN, J. R., MEASE, K. D., and HANSON, J.M., Explicit Guidance of Drag-Modulated Aeroassisted Transfer between Elliptical Orbits, Journal of Guidance, Control, and Dynamics, Vol. 9, No. 2, pp. 274-280, 1986.

9. MEASE, K. D., and McCREARY, F. A., Atmospheric Guidance Law for Planar Skip Trajectories, Paper No. AIAA-85-1818, AIAA 12th Atmospheric Flight Mechanics Conference, Snowmass, Colorado, 1985.

10. LEE, B. S., and GRANTHAM, W. J., Aeroassisted Orbital Maneuvering Using Lyapunov Optimal Feedback Control, Journal of Guidance, Control, and Dynamics, Vol. 12, No. 2, pp. 237-242, 1989.

11. GAMBLE, J.D., CERIMELE, C. J., MOORE, T. E., and HIGGINS, J., Atmospheric Guidance Concepts for an Aeroassist Flight Experiment, Journal of the Astronautical Sciences, Vol. 36, Nos. 1-2, pp. 45-71, 1988.

12. MIELE, A., WANG, T., and LEE, W. Y., Optimization and Guidance of Trajectories for Coplanar, Aeroassisted Orbital Transfer, Rice University, Aero-Astronautics Report No. 241, 1989.

13. MIELE, A., WANG, T., TZENG, C. Y., and MELVIN, W. W., Abort Landing Guidance Trajectories in the Presence of Windshear, Journal of the Franklin Institute, Vol. 326, No. 2, pp. 185-220, 1989.

14. MIELE, A., WANG, T., MELVIN, W. W., and BOWLES, R. L., Acceleration, Gamma, and Theta Guidance for Abort Landing in a Windshear, Journal of Guidance, Control, and Dynamics, Vol. 12, No. 6, pp. 815-821, 1989.

15. NOAA, NASA, and USAF, US Standard Atmosphere, 1976, US Government Printing Office, Washington, DC, 1976.

16. MIELE, A., WANG, T., and BASAPUR, V. K., Primal and Dual Formulations of Sequential Gradient-Restoration Algorithms for Trajectory Optimization Problems, Acta Astronautica, Vol. 13, No. 8, pp. 491-505, 1986.

17. MIELE, A., and WANG, T., Primal-Dual Properties of Sequential Gradient-Restoration Algorithms for Optimal Control Problems, Part 1, Basic Problem, Integral Methods in Science and Engineering, Edited by F. R. Payne et al, Hemisphere Publishing Corporation, Washington, DC, pp. 577-607, 1986.

18. MIELE, A., and WANG, T., Primal-Dual Properties of Sequential Gradient-Restoration Algorithms for Optimal Control Problems, Part 2, General Problem, Journal of Mathematical Analysis and Applications, Vol. 119, Nos. 1-2, pp. 21-54, 1986.

List of Tables

List of Captions

Fig. 1. Coplanar, aeroassisted orbital transfer.

Fig. 2A. Optimal trajectories,
altitude h versus time t.

Fig. 2B. Optimal trajectories,
velocity V versus time t.

Fig. 2C. Optimal trajectories,
path inclination γ versus time t.

Fig. 2D. Optimal trajectories,
lift coefficient C_L versus time t.

Fig. 3A. Optimal trajectories, descending branch,
normalized path inclination versus normalized altitude.

Fig. 3B. Optimal trajectories, ascending branch,
normalized path inclination versus normalized altitude.

Fig. 4A. Trajectory comparison, Case 1,
altitude h versus time t.

Fig. 4B. Trajectory comparison, Case 1,
velocity V versus time t.

Fig. 4C. Trajectory comparison, Case 1,
path inclination γ versus time t.

Fig. 4D. Trajectory comparison, Case 1,
lift coefficient C_L versus time t.

Fig. 5A. Trajectory comparison, Case 2,
altitude h versus time t.

Fig. 5B. Trajectory comparison, Case 2,
velocity V versus time t.

Fig. 8C. Modified gamma guidance trajectories, effect of change in the zero-lift drag.

Fig. 8D. Modified gamma guidance trajectories, effect of change in the induced drag.

Fig. 8E. Modified gamma guidance trajectories, effect of change in the lift range.

Table 1. Results for the optimal trajectories.

Quantity	Case 1	Case 2	Case 3	Units
h_0	120.0	120.0	120.0	km
V_0	9.040	9.905	10.310	km/sec
γ_0	-3.034	-3.893	-4.204	deg
h_1	120.0	120.0	120.0	km
V_1	7.844	7.844	7.844	km/sec
γ_1	0.319	0.319	0.319	deg
h_{min}	79.50	76.35	75.36	km
PHR	35.90	59.61	72.70	W/cm^2
τ	2.147	2.297	2.347	ksec
ΔV_{00}	1.025	1.445	1.490	km/sec
ΔV_1	0.000	0.000	0.000	km/sec
ΔV_{11}	0.025	0.025	0.025	km/sec
ΔV	1.049	1.470	1.515	km/sec

Table 2. Comparison of characteristic velocities ΔV(km/sec).

Trajectory	Case 1	Case 2	Case 3
Optimal	1.049	1.470	1.515
Grazing	1.034	1.457	1.504
Hohmann	2.195	3.486	3.940

Table 3. Parameters of gamma guidance trajectories.

Quantity	Case 1	Case 2	Case 3	Units
γ_0	-3.300	-4.100	-4.400	deg
h_T	78.25	75.75	74.32	km
V_S	8.700	9.180	9.400	km/sec
γ_T	0.115	0.113	0.114	deg
C_{LT}	-0.270	-0.270	-0.288	-
A	0.716	0.648	0.632	-
B	0.361	0.354	0.357	-

Table 4. Results for gamma guidance trajectories.

Quantity	Case 1	Case 2	Case 3	Units
h_0	120.0	120.0	120.0	km
V_0	9.039	9.905	10.310	km/sec
γ_0	-3.300	-4.100	-4.400	deg
h_1	120.0	120.0	120.0	km
V_1	7.832	7.834	7.841	km/sec
γ_1	0.187	0.217	0.300	deg
h_{min}	78.29	75.73	74.28	km
PHR	39.29	62.44	78.27	W/cm^2
τ	2.456	2.527	2.405	ksec
ΔV_{00}	1.026	1.446	1.490	km/sec
ΔV_1	0.016	0.013	0.003	km/sec
ΔV_{11}	0.020	0.021	0.024	km/sec
ΔV	1.063	1.480	1.517	km/sec

Table 5. Comparison of characteristic velocities ΔV(km/sec).

Trajectory	Case 1	Case 2	Case 3
OT	1.049	1.470	1.515
GGT	1.063	1.480	1.517

Table 6. Comparison of results, Case 1.

Quantity	OT	GGT	Units
h_0	120.0	120.0	km
V_0	9.040	9.039	km/sec
γ_0	-3.034	-3.300	deg
h_1	120.0	120.0	km
V_1	7.844	7.832	km/sec
γ_1	0.319	0.187	deg
h_{min}	79.50	78.29	km
PHR	35.90	39.29	W/cm^2
τ	2.147	2.456	ksec
ΔV_{00}	1.025	1.026	km/sec
ΔV_1	0.000	0.016	km/sec
ΔV_{11}	0.025	0.020	km/sec
ΔV	1.049	1.063	km/sec

Table 7. Comparison of results, Case 2.

Quantity	OT	GGT	Units
h_0	120.0	120.0	km
V_0	9.905	9.905	km/sec
γ_0	-3.893	-4.100	deg
h_1	120.0	120.0	km
V_1	7.844	7.834	km/sec
γ_1	0.319	0.217	deg
h_{min}	76.35	75.73	km
PHR	59.61	62.44	W/cm^2
τ	2.297	2.527	ksec
ΔV_{00}	1.445	1.446	km/sec
ΔV_1	0.000	0.013	km/sec
ΔV_{11}	0.025	0.021	km/sec
ΔV	1.470	1.480	km/sec

Table 8. Comparison of results, Case 3.

Quantity	OT	GGT	Units
h_0	120.0	120.0	km
V_0	10.310	10.310	km/sec
γ_0	-4.204	-4.400	deg
h_1	120.0	120.0	km
V_1	7.844	7.841	km/sec
γ_1	0.319	0.300	deg
h_{min}	75.36	74.28	km
PHR	72.70	78.27	W/cm^2
τ	2.347	2.405	ksec
ΔV_{00}	1.490	1.490	km/sec
ΔV_1	0.000	0.003	km/sec
ΔV_{11}	0.025	0.024	km/sec
ΔV	1.515	1.517	km/sec

Table 9. Parameters of modified gamma guidance trajectories, Case 3.

Quantity	GGT	MGGT	Units
γ_0	-4.400	-4.500	deg
h_T	74.32	71.14	km
V_S	9.400	8.400	km/sec
γ_T	0.114	0.150	deg
C_{LT}	-0.288	-0.180	-
A	0.632	0.225	-
B	0.357	0.470	-

$F_{\gamma 0} = 1$, $F_\rho = 1$, $F_{CD0} = 1$, $F_K = 1$, $F_{CLR} = 1$.

Table 10. Results for modified gamma guidance trajectories, Case 3.

Quantity	GGT	MGGT	Units
h_0	120.0	120.0	km
V_0	10.310	10.310	km/sec
γ_0	-4.400	-4.500	deg
h_1	120.0	120.0	km
V_1	7.841	7.835	km/sec
γ_1	0.300	0.245	deg
h_{min}	74.28	71.14	km
PHR	78.27	96.97	W/cm^2
τ	2.405	3.012	ksec
ΔV_{00}	1.490	1.491	km/sec
ΔV_1	0.003	0.011	km/sec
ΔV_{11}	0.024	0.022	km/sec
ΔV	1.517	1.523	km/sec

$F_{\gamma 0} = 1$, $F_\rho = 1$, $F_{CD0} = 1$, $F_K = 1$, $F_{CLR} = 1$.

Table 11A. Effect of path inclination factor F_{γ_0}, Case 3, modified gamma guidance trajectories.

F_{γ_0}	γ_0 deg	h_T km	V_S km/sec	γ_T deg	C_{LT}	A	B
0.91	-4.1	71.14	8.4	0.15	-0.18	0.225	0.470
0.96	-4.3	71.14	8.4	0.15	-0.18	0.225	0.470
1.00	-4.5	71.14	8.4	0.15	-0.18	0.225	0.470
1.11	-5.0	71.14	8.4	0.15	-0.18	0.225	0.470
1.22	-5.5	71.14	8.4	0.15	-0.18	0.225	0.470
1.44	-6.5	71.14	8.4	0.15	-0.18	0.225	0.470

Table 11B. Effect of path inclination factor $F_{\gamma 0}$, Case 3, modified gamma guidance trajectories.

$F_{\gamma 0}$	h_0 km	V_0 km/sec	γ_0 deg	h_1 km	V_1 km/sec	γ_1 deg
0.91	120.0	10.310	-4.1	120.0	7.835	0.244
0.96	120.0	10.310	-4.3	120.0	7.836	0.245
1.00	120.0	10.310	-4.5	120.0	7.835	0.245
1.11	120.0	10.310	-5.0	120.0	7.835	0.244
1.22	120.0	10.309	-5.5	120.0	7.836	0.245
1.44	120.0	10.309	-6.5	120.0	7.835	0.243

Table 11C. Effect of path inclination factor $F_{\gamma 0}$, Case 3, modified gamma guidance trajectories.

$F_{\gamma 0}$	h_{min} km	PHR W/cm^2	τ ksec	ΔV_{00} km/sec	ΔV_1 km/sec	ΔV_{11} km/sec	ΔV km/sec
0.91	71.14	83.79	2.986	1.490	0.011	0.022	1.523
0.96	71.14	93.33	3.010	1.490	0.011	0.022	1.523
1.00	71.14	96.97	3.012	1.491	0.011	0.022	1.523
1.11	69.67	113.45	2.982	1.492	0.011	0.022	1.525
1.22	66.43	136.61	2.927	1.493	0.011	0.022	1.526
1.44	60.91	180.80	2.810	1.496	0.011	0.022	1.529

Table 12A. Effect of density factor F_ρ, Case 3, modified gamma guidance trajectories.

F_ρ	γ_0 deg	h_T km	V_S km/sec	γ_T deg	C_{LT}	A	B
0.33	-4.5	62.98	8.4	0.15	-0.18	0.225	0.470
0.50	-4.5	66.13	8.4	0.15	-0.18	0.225	0.470
1.00	-4.5	71.14	8.4	0.15	-0.18	0.225	0.470
2.00	-4.5	75.79	8.4	0.15	-0.18	0.225	0.470
3.00	-4.5	78.41	8.4	0.15	-0.18	0.225	0.470
5.00	-4.5	81.63	8.4	0.15	-0.18	0.225	0.470
10.00	-4.5	85.84	8.4	0.15	-0.18	0.225	0.470

Table 12B. Effect of density factor F_ρ, Case 3, modified gamma guidance trajectories.

F_ρ	h_0 km	V_0 km/sec	γ_0 deg	h_1 km	V_1 km/sec	γ_1 deg
0.33	120.0	10.310	-4.5	120.0	7.824	0.116
0.50	120.0	10.310	-4.5	120.0	7.828	0.175
1.00	120.0	10.310	-4.5	120.0	7.835	0.245
2.00	120.0	10.310	-4.5	120.0	7.842	0.273
3.00	120.0	10.310	-4.5	120.0	7.845	0.276
5.00	120.0	10.310	-4.5	120.0	7.849	0.267
10.00	120.0	10.310	-4.5	120.0	7.853	0.241

Table 12C. Effect of density factor F_ρ, Case 3, modified gamma guidance trajectories.

F_ρ	h_{min} km	PHR W/cm^2	τ ksec	ΔV_{00} km/sec	ΔV_1 km/sec	ΔV_{11} km/sec	ΔV km/sec
0.33	62.98	87.66	3.670	1.491	0.025	0.019	1.535
0.50	66.13	91.36	3.366	1.491	0.020	0.020	1.531
1.00	71.14	96.97	3.012	1.491	0.011	0.022	1.523
2.00	75.52	103.99	2.773	1.491	0.003	0.023	1.517
3.00	77.67	109.09	2.660	1.491	0.000	0.023	1.514
5.00	80.08	116.50	2.535	1.491	0.003	0.023	1.516
10.00	83.11	127.67	2.376	1.491	0.007	0.022	1.519

Table 13A. Effect of zero-lift drag factor F_{CD0}, Case 3, modified gamma guidance trajectories.

F_{CD0}	γ_0 deg	h_T km	V_S km/sec	γ_T deg	C_{LT}	A	B
0.10	-4.5	71.14	8.20	0.15	-0.18	0.144	0.470
0.20	-4.5	71.14	8.25	0.15	-0.18	0.165	0.470
0.50	-4.5	71.14	8.35	0.15	-0.18	0.205	0.470
1.00	-4.5	71.14	8.40	0.15	-0.18	0.225	0.470
2.00	-4.5	71.14	8.50	0.15	-0.18	0.266	0.470
5.00	-4.5	71.14	9.10	0.21	-0.18	0.509	0.658

Table 13B. Effect of zero-lift drag factor F_{CD0}, Case 3, modified gamma guidance trajectories.

F_{CD0}	h_0 km	V_0 km/sec	γ_0 deg	h_1 km	V_1 km/sec	γ_1 deg
0.10	120.0	10.310	-4.5	120.0	7.861	0.462
0.20	120.0	10.310	-4.5	120.0	7.863	0.476
0.50	120.0	10.310	-4.5	120.0	7.859	0.447
1.00	120.0	10.310	-4.5	120.0	7.835	0.245
2.00	120.0	10.310	-4.5	120.0	7.823	0.114
5.00	120.0	10.310	-4.5	120.0	7.825	0.197

Table 13C. Effect of zero-lift drag factor F_{CD0}, Case 3, modified gamma guidance trajectories.

F_{CD0}	h_{min} km	PHR W/cm^2	τ ksec	ΔV_{00} km/sec	ΔV_1 km/sec	ΔV_{11} km/sec	ΔV km/sec
0.10	71.14	98.96	4.268	1.491	0.025	0.032	1.547
0.20	71.14	98.73	3.686	1.491	0.028	0.033	1.551
0.50	71.14	98.05	3.043	1.491	0.022	0.031	1.543
1.00	71.14	96.97	3.012	1.491	0.011	0.022	1.523
2.00	71.14	94.98	3.024	1.491	0.026	0.019	1.536
5.00	71.14	90.00	1.953	1.491	0.022	0.020	1.534

Table 14A. Effect of induced drag factor F_K, Case 3, modified gamma guidance trajectories.

F_K	γ_0 deg	h_T km	V_S km/sec	γ_T deg	C_{LT}	A	B
0.10	-4.5	71.14	8.15	0.15	-0.18	0.124	0.470
0.20	-4.5	71.14	8.15	0.15	-0.18	0.124	0.470
0.50	-4.5	71.14	8.25	0.15	-0.18	0.165	0.470
1.00	-4.5	71.14	8.40	0.15	-0.18	0.225	0.470
2.00	-4.5	71.14	8.40	0.15	-0.18	0.225	0.470
5.00	-4.5	71.14	9.10	0.25	-0.18	0.509	0.784

Table 14B. Effect of induced drag factor F_K, Case 3, modified gamma guidance trajectories.

F_K	h_0 km	V_0 km/sec	γ_0 deg	h_1 km	V_1 km/sec	γ_1 deg
0.10	120.0	10.310	-4.5	120.0	7.836	0.218
0.20	120.0	10.310	-4.5	120.0	7.832	0.173
0.50	120.0	10.310	-4.5	120.0	7.863	0.456
1.00	120.0	10.310	-4.5	120.0	7.835	0.245
2.00	120.0	10.310	-4.5	120.0	7.822	0.110
5.00	120.0	10.310	-4.5	120.0	7.818	0.213

Table 14C. Effect of induced drag factor F_K, Case 3, modified gamma guidance trajectories.

F_K	h_{min} km	PHR W/cm^2	τ ksec	ΔV_{00} km/sec	ΔV_1 km/sec	ΔV_{11} km/sec	ΔV km/sec
0.10	71.14	103.63	4.281	1.491	0.011	0.021	1.523
0.20	71.14	102.66	4.183	1.491	0.016	0.020	1.527
0.50	71.14	100.19	3.186	1.491	0.026	0.031	1.548
1.00	71.14	96.97	3.012	1.491	0.011	0.022	1.523
2.00	71.14	92.33	3.072	1.491	0.027	0.019	1.537
5.00	71.21	83.95	1.646	1.491	0.029	0.021	1.541

Table 15A. Effect of lift range factor F_{CLR}, Case 3, modified gamma guidance trajectories.

F_{CLR}	γ_0 deg	h_T km	V_S km/sec	γ_T deg	C_{LT}	A	B
0.33	-4.5	62.98	9.0	0.15	-0.059	0.469	0.470
0.50	-4.5	66.13	8.5	0.15	-0.090	0.266	0.470
1.00	-4.5	71.14	8.4	0.15	-0.180	0.225	0.470
2.00	-4.5	75.79	8.4	0.15	-0.360	0.225	0.470
3.00	-4.5	78.41	8.4	0.15	-0.540	0.225	0.470

Table 15B. Effect of lift range factor F_{CLR}, Case 3, modified gamma guidance trajectories.

F_{CLR}	h_0 km	V_0 km/sec	γ_0 deg	h_1 km	V_1 km/sec	γ_1 deg
0.33	120.0	10.310	-4.5	120.0	7.861	0.524
0.50	120.0	10.310	-4.5	120.0	7.821	0.055
1.00	120.0	10.310	-4.5	120.0	7.835	0.245
2.00	120.0	10.310	-4.5	120.0	7.827	0.145
3.00	120.0	10.310	-4.5	120.0	7.825	0.146

Table 15C. Effect of lift range factor F_{CLR}, Case 3, modified gamma guidance trajectories.

F_{CLR}	h_{min} km	PHR W/cm^2	τ ksec	ΔV_{00} km/sec	ΔV_1 km/sec	ΔV_{11} km/sec	ΔV km/sec
0.33	61.50	174.29	2.390	1.491	0.029	0.036	1.555
0.50	64.41	157.37	3.567	1.491	0.029	0.018	1.538
1.00	71.14	96.97	3.012	1.491	0.011	0.022	1.523
2.00	75.79	62.44	2.879	1.491	0.022	0.019	1.532
3.00	78.41	49.08	2.571	1.491	0.023	0.019	1.533

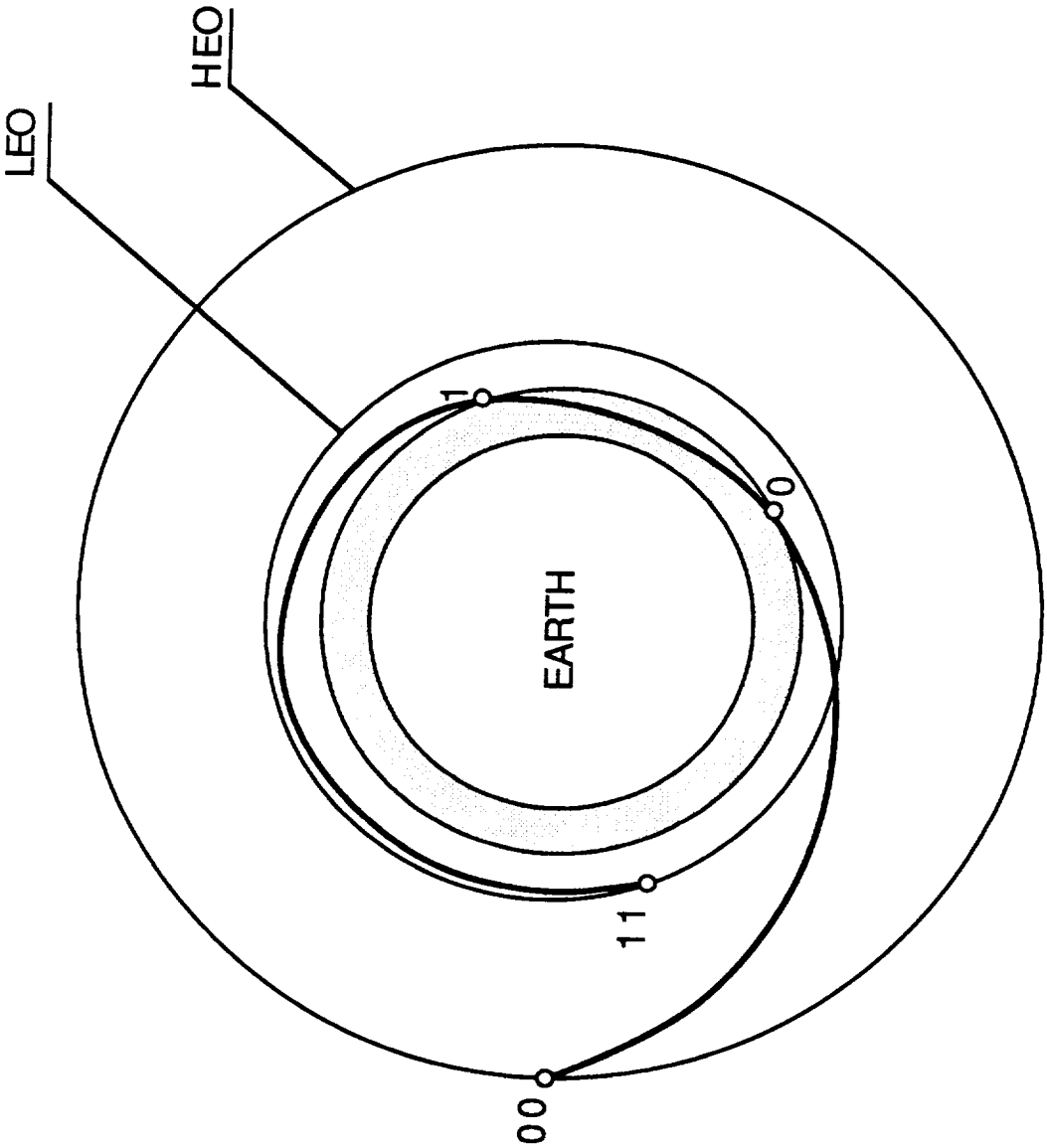

Fig.1. Coplanar, aeroassisted orbital transfer.

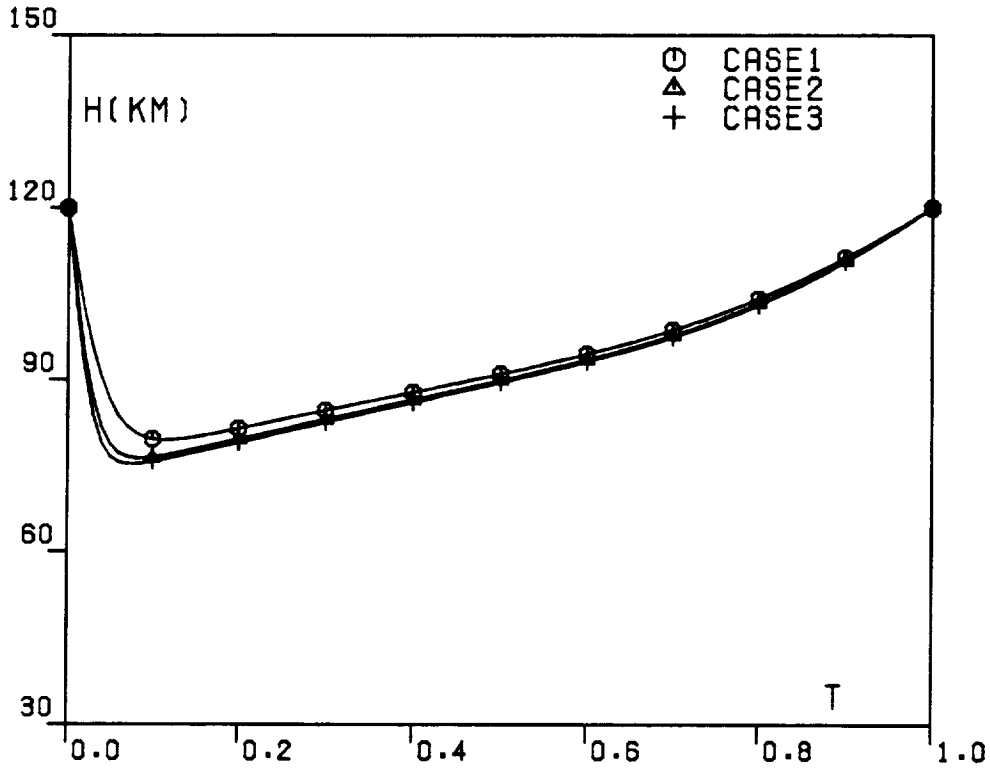

FIG. 2A. OPTIMAL TRAJECTORIES.

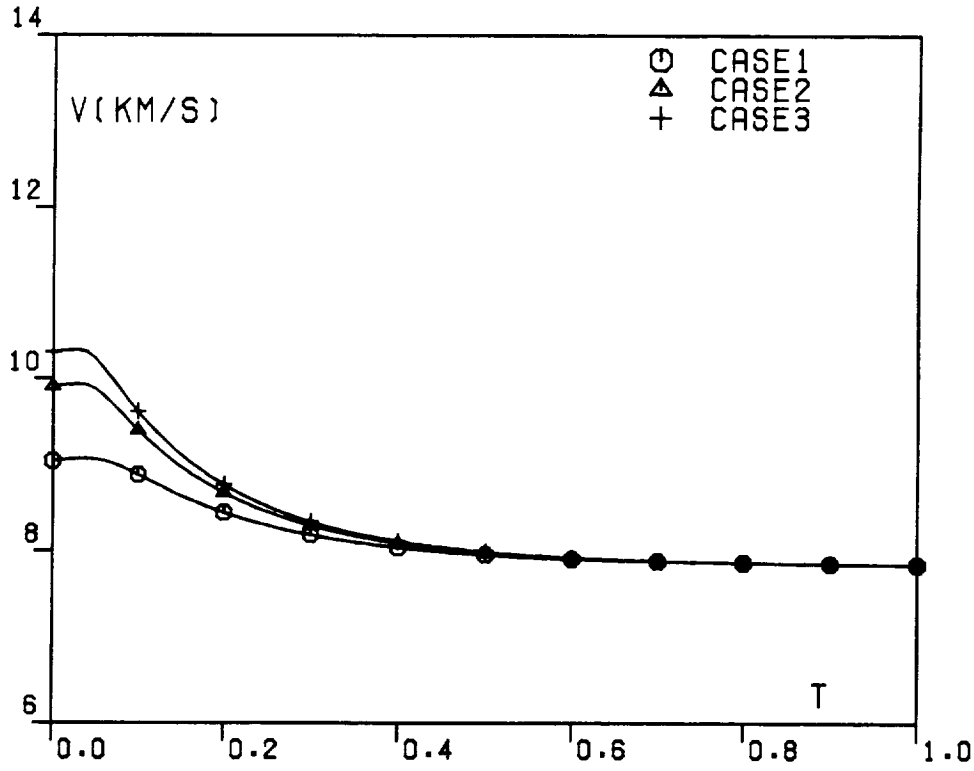

FIG. 2B. OPTIMAL TRAJECTORIES.

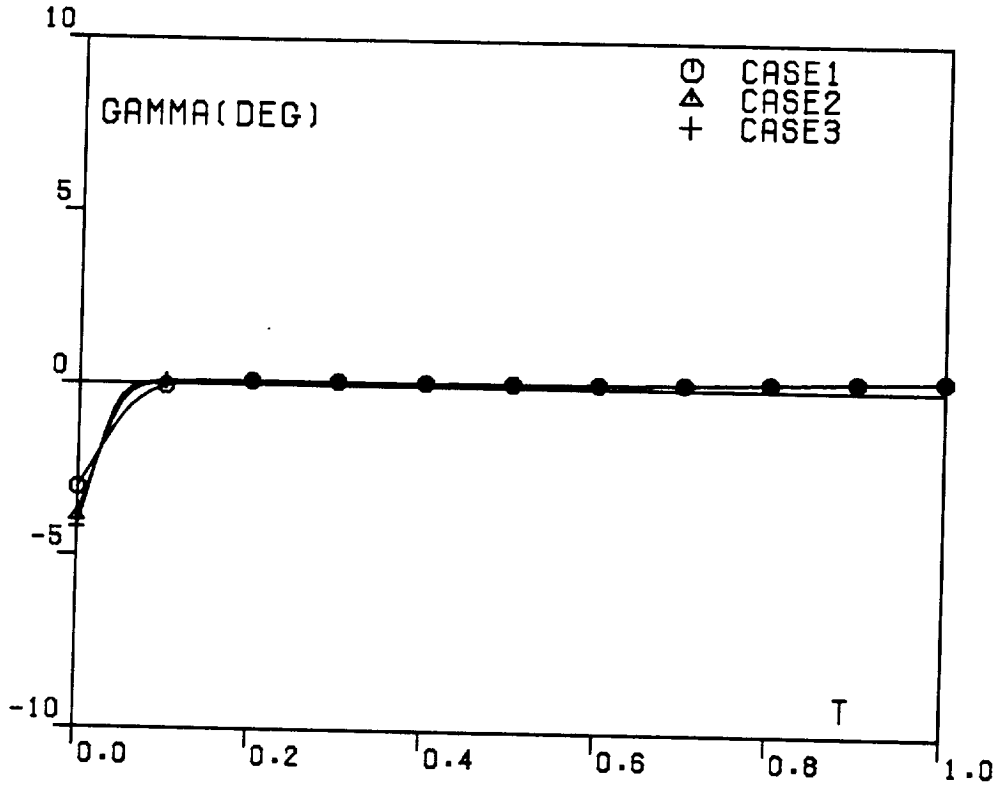

FIG. 2C. OPTIMAL TRAJECTORIES.

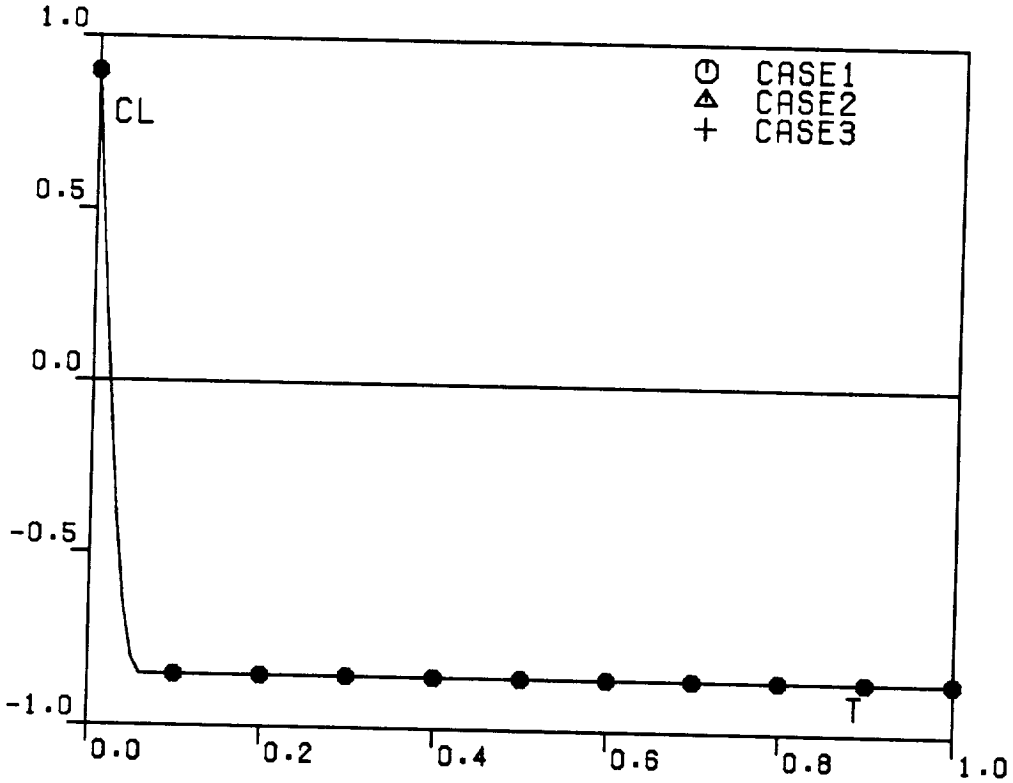

FIG. 2D. OPTIMAL TRAJECTORIES.

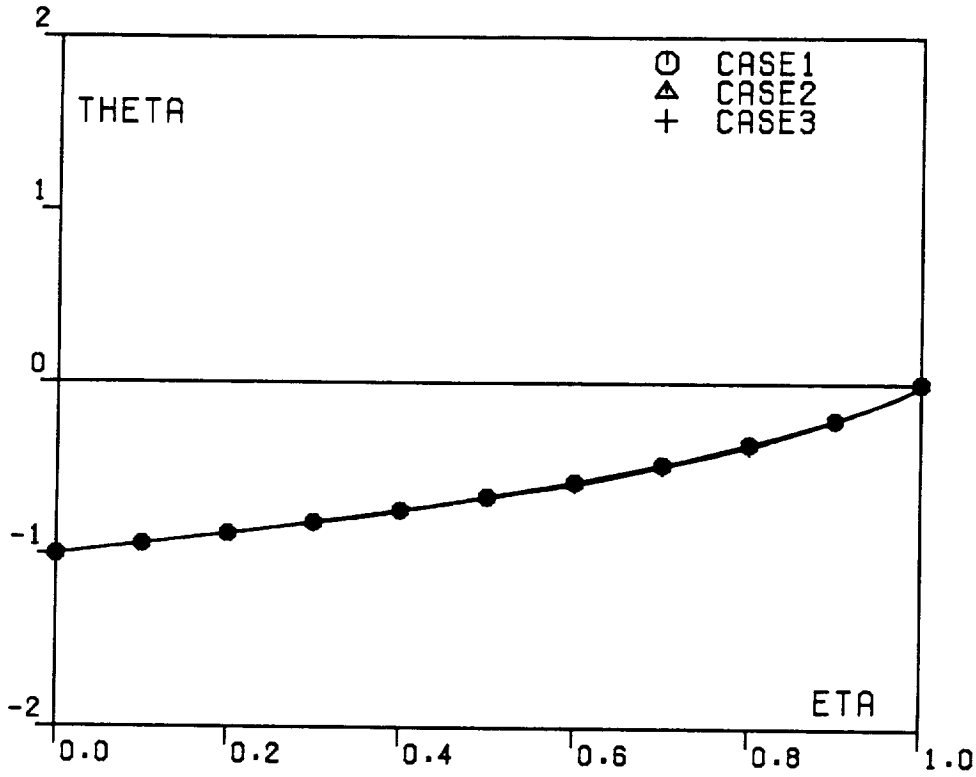

FIG. 3A. OPTIMAL TRAJECTORIES, BRANCH 1.

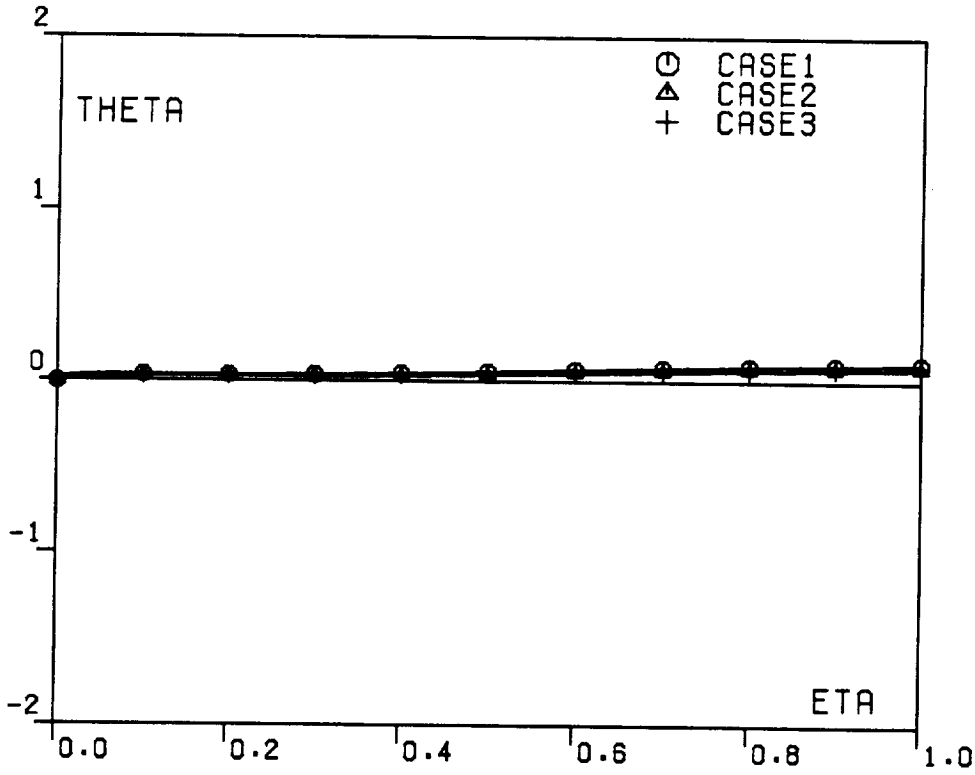

FIG. 3B. OPTIMAL TRAJECTORIES, BRANCH 2.

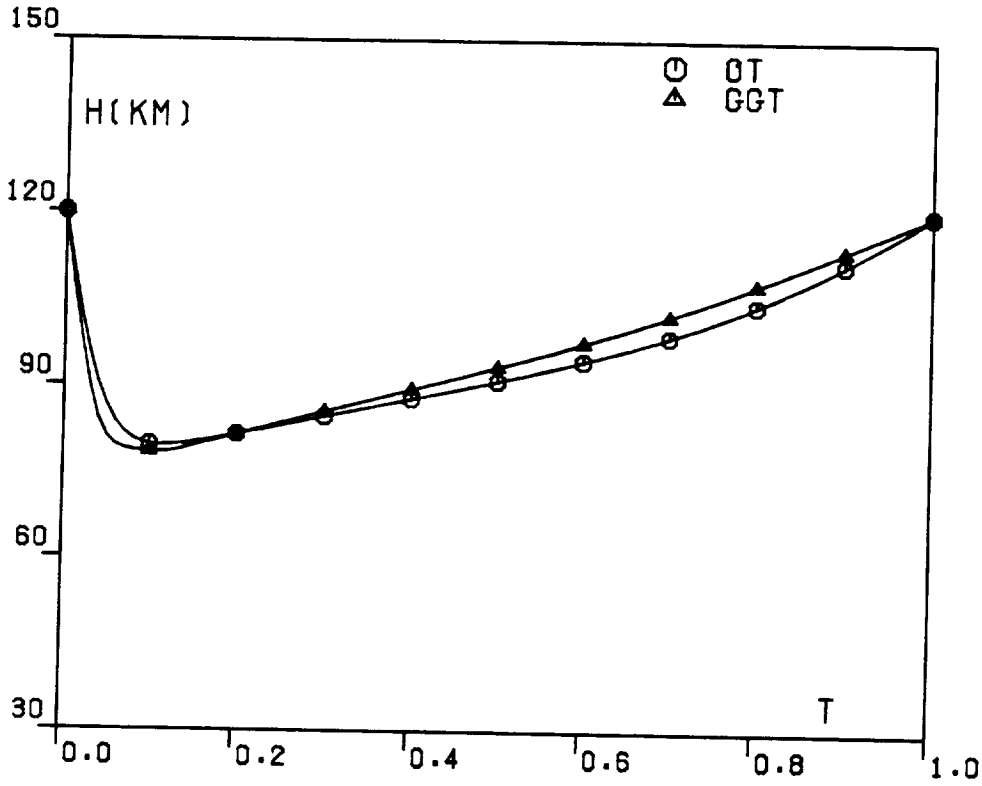

FIG. 4A. TRAJECTORY COMPARISON, CASE1.

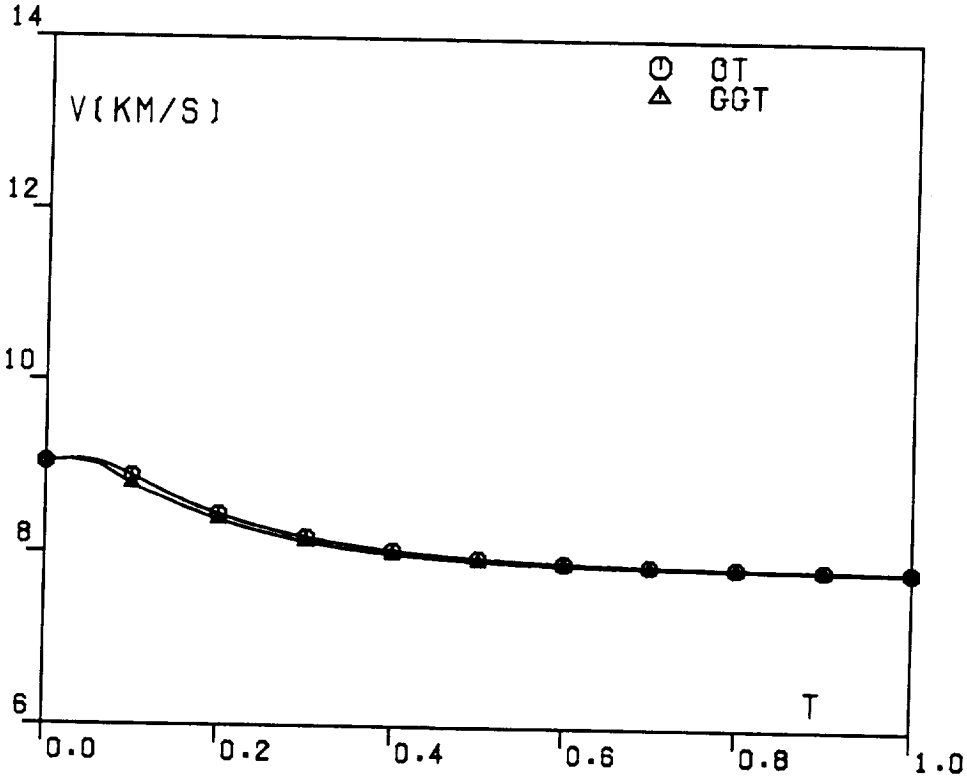

FIG. 4B. TRAJECTORY COMPARISON, CASE1.

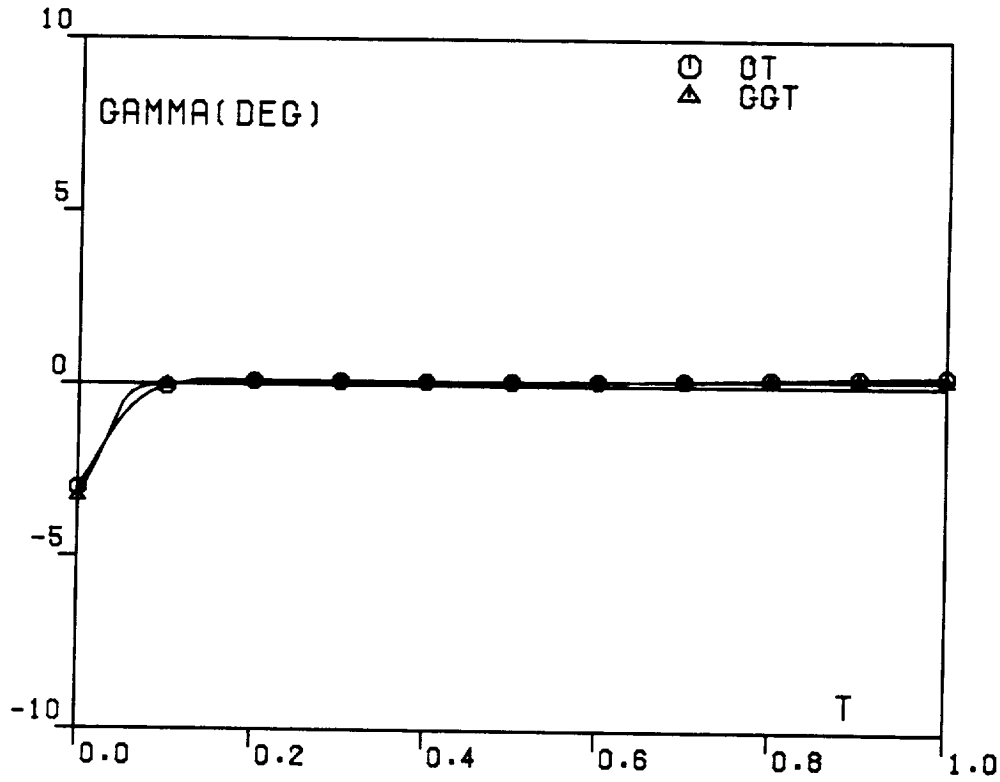

FIG. 4C. TRAJECTORY COMPARISON, CASE1.

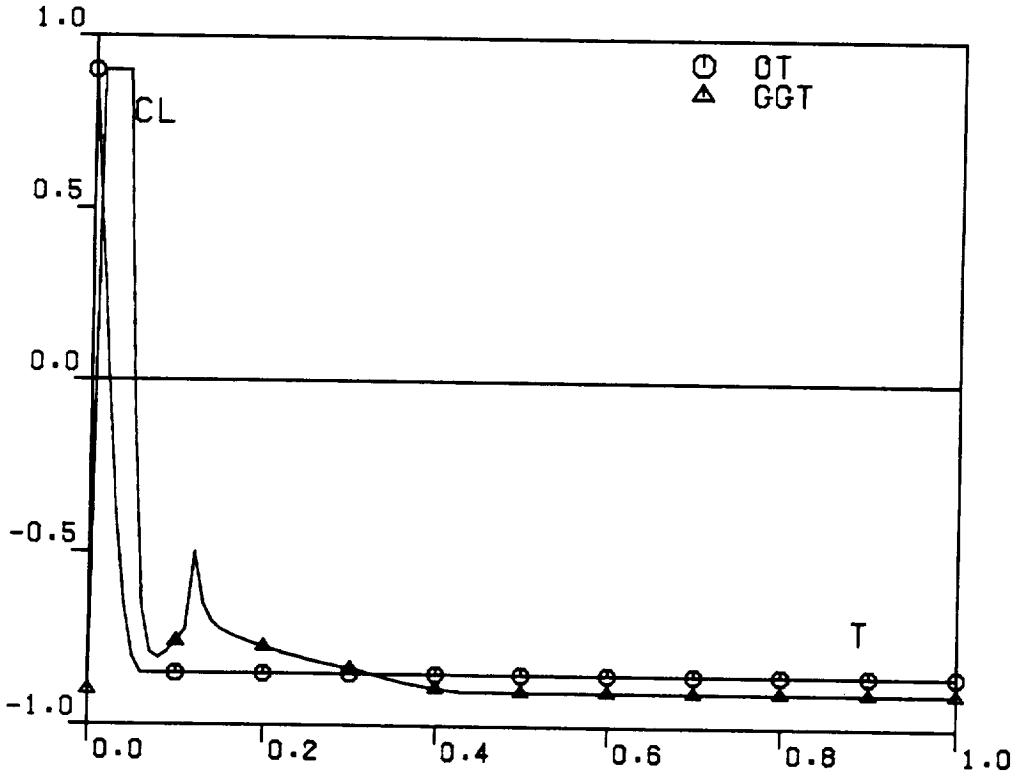

FIG. 4D. TRAJECTORY COMPARISON, CASE1.

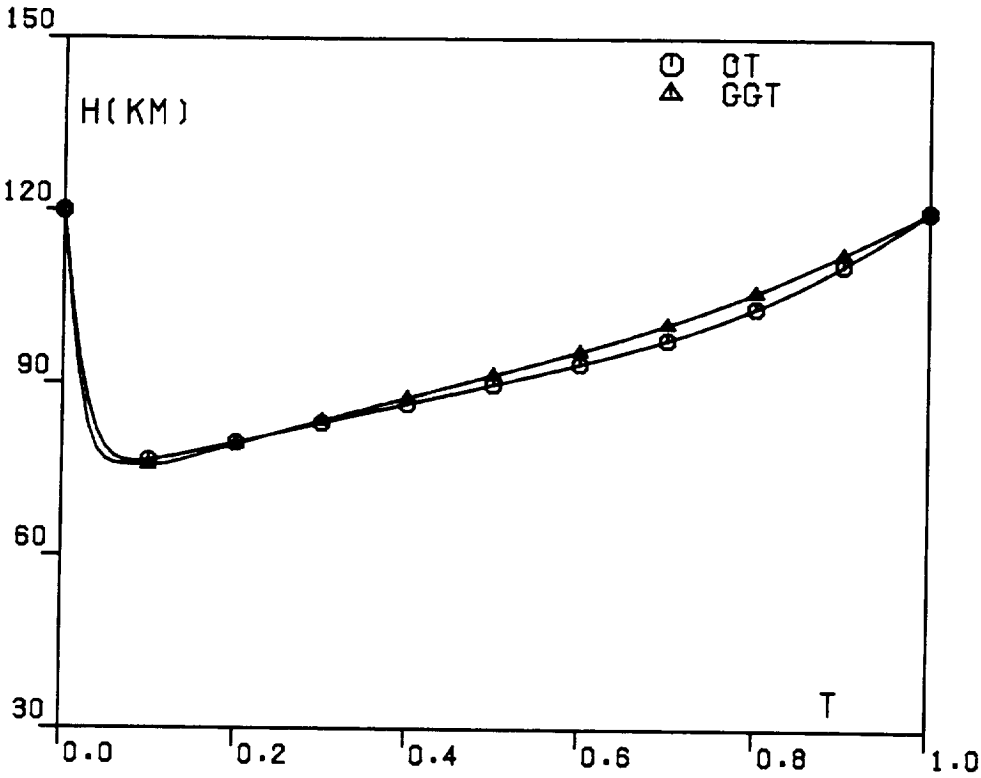

FIG. 5A. TRAJECTORY COMPARISON, CASE2.

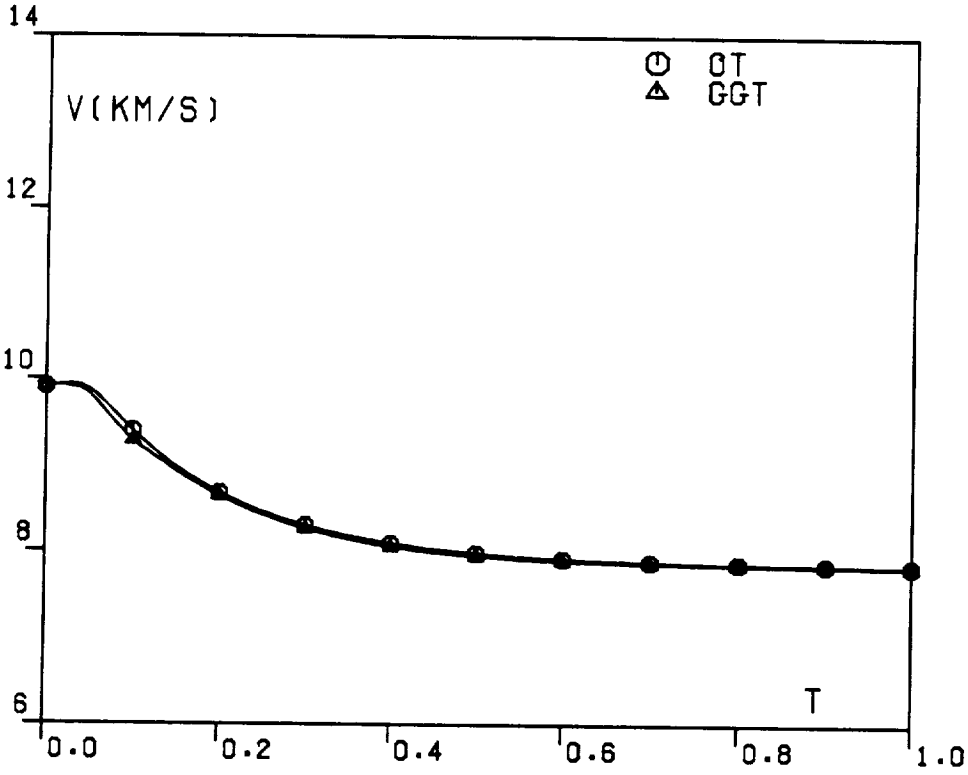

FIG. 5B. TRAJECTORY COMPARISON, CASE2.

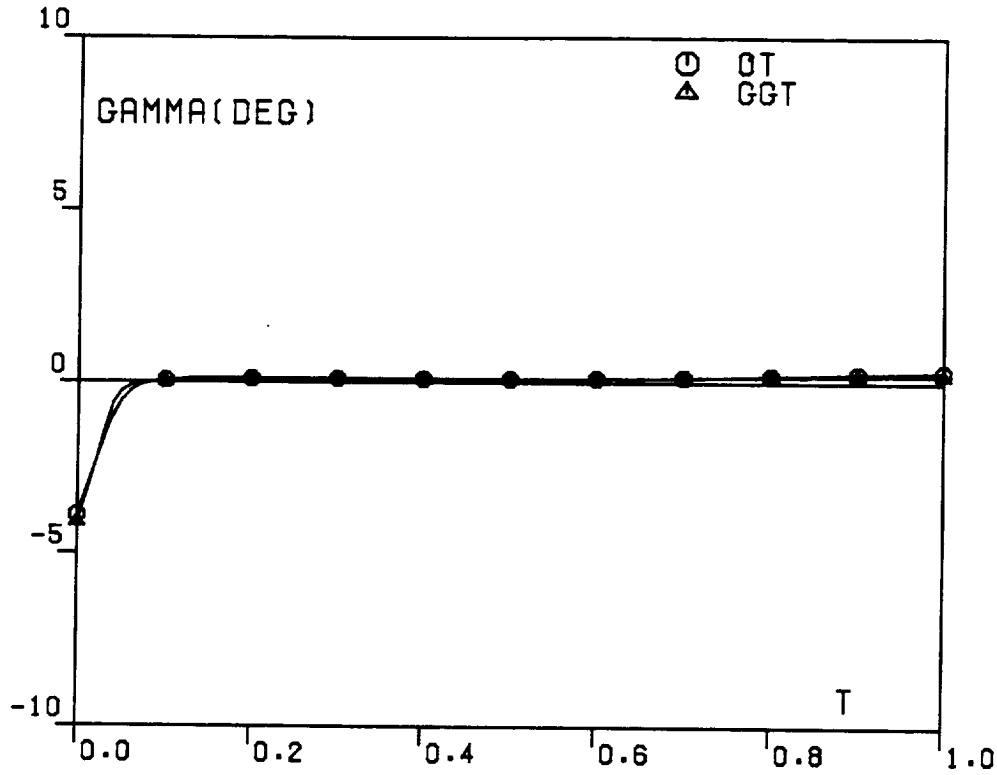

FIG. 5C. TRAJECTORY COMPARISON, CASE2.

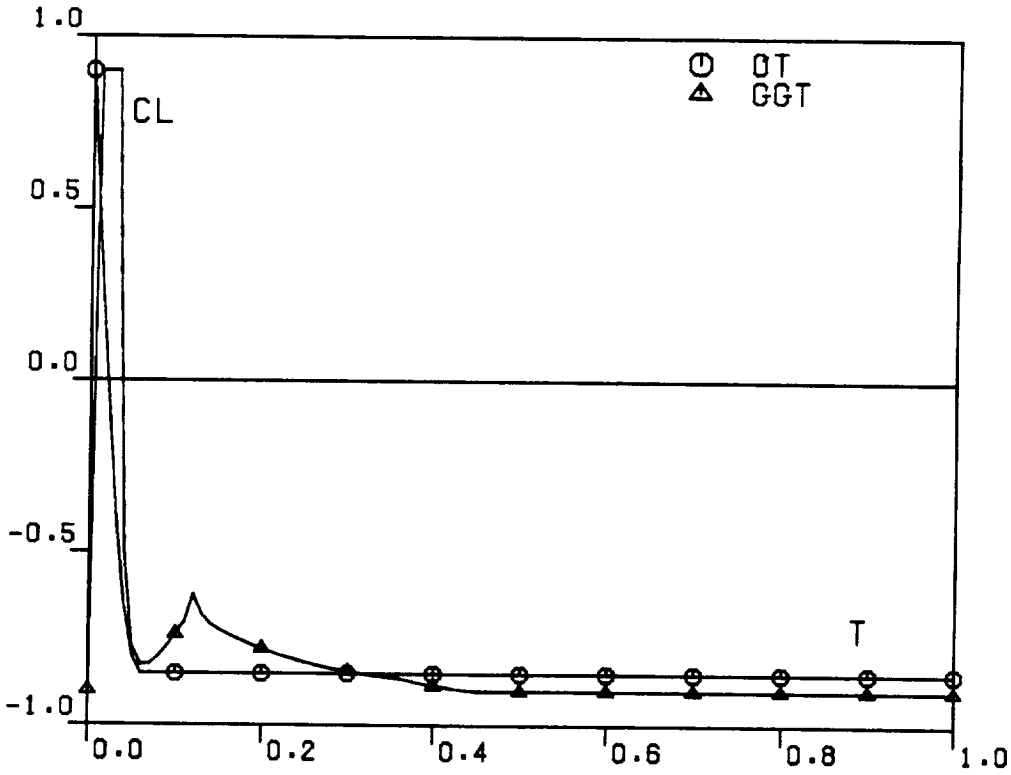

FIG. 5D. TRAJECTORY COMPARISON, CASE2.

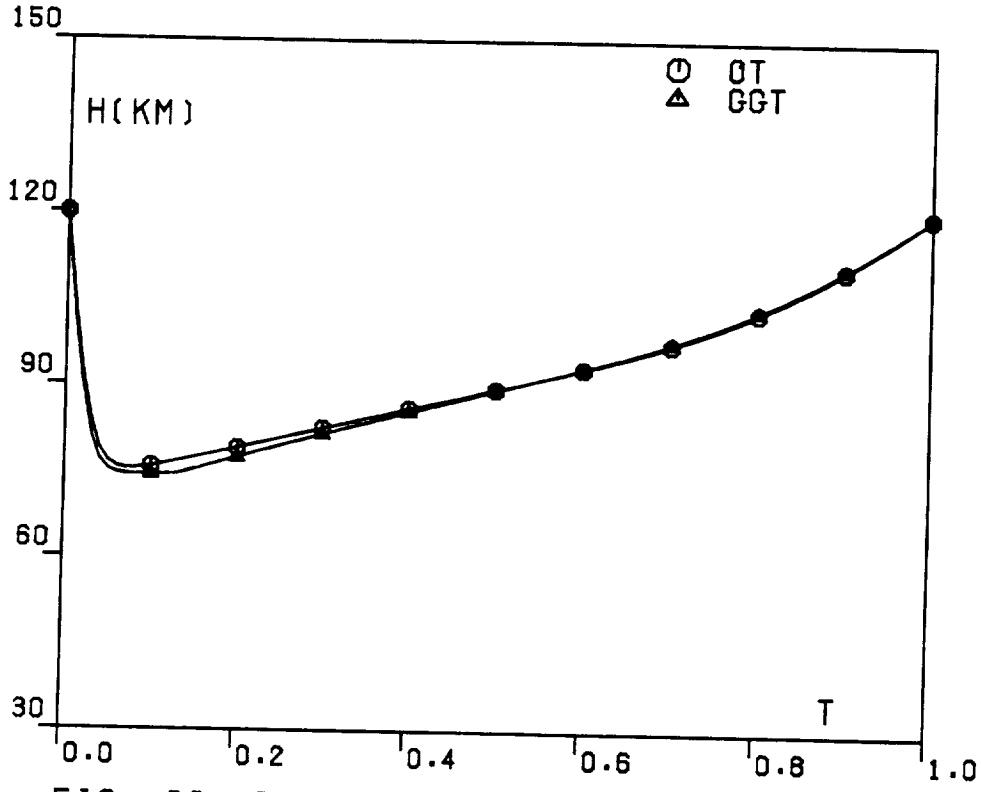

FIG. 6A. TRAJECTORY COMPARISON, CASE3.

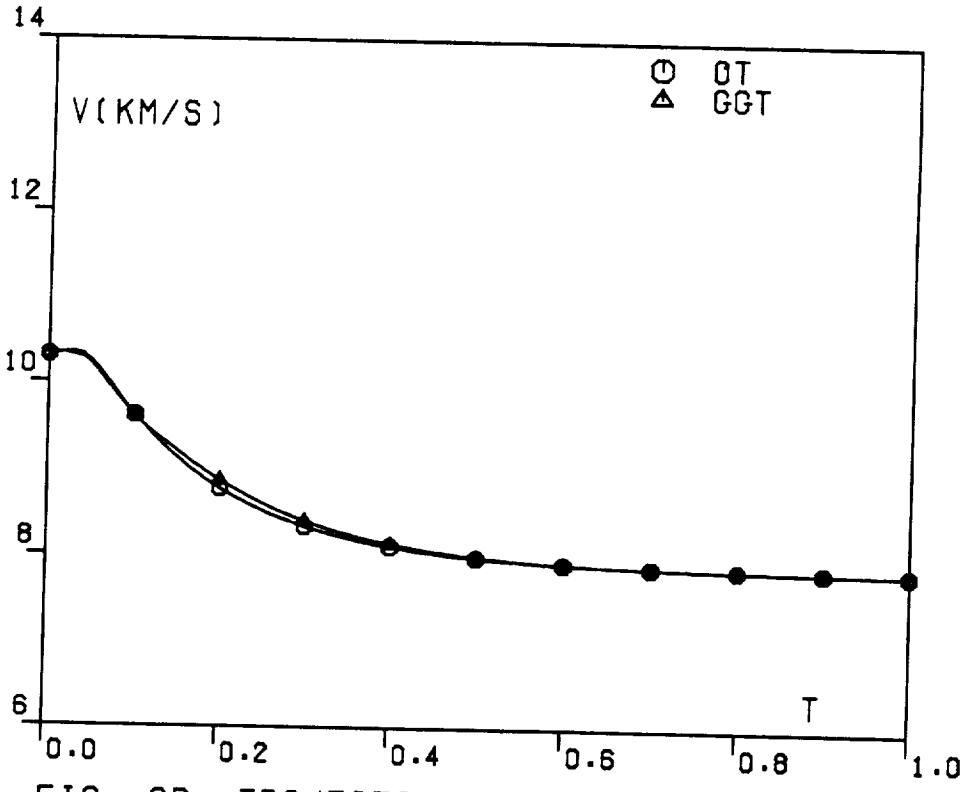

FIG. 6B. TRAJECTORY COMPARISON, CASE3.

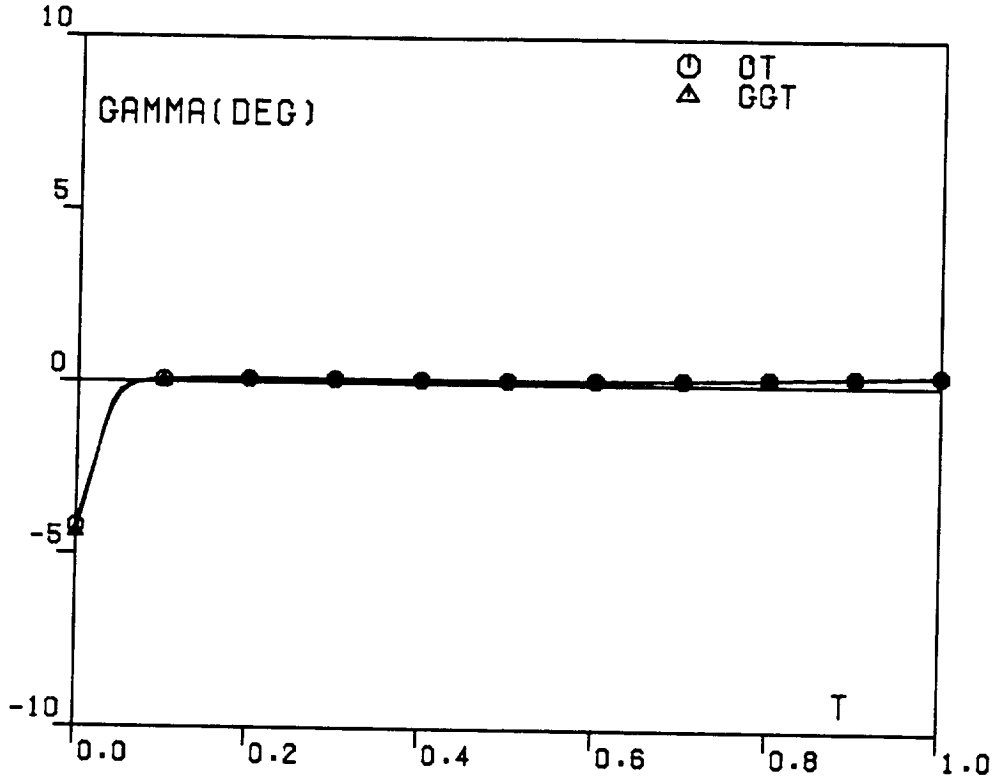

FIG. 6C. TRAJECTORY COMPARISON, CASE3.

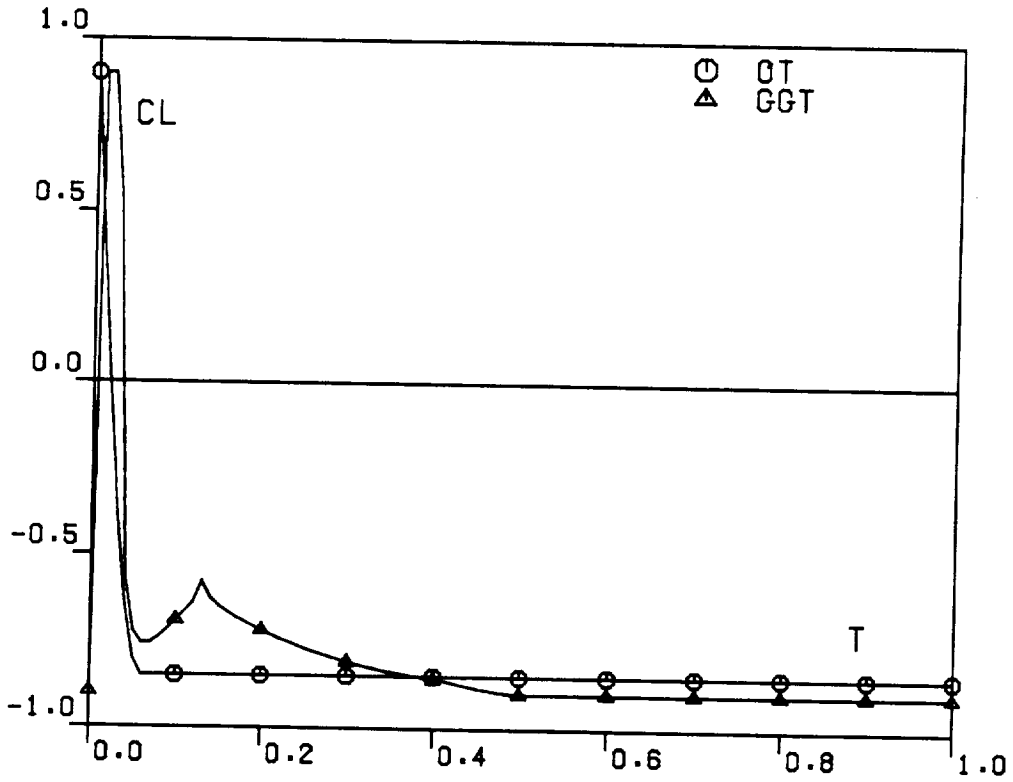

FIG. 6D. TRAJECTORY COMPARISON, CASE3.

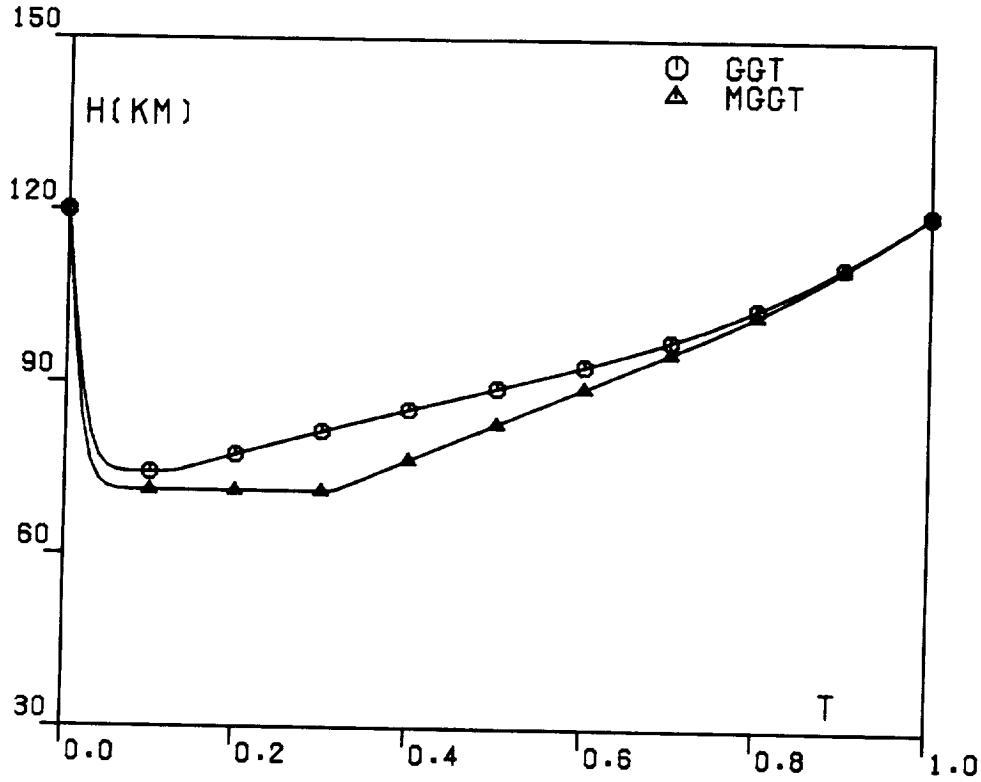

FIG. 7A. TRAJECTORY COMPARISON, CASE3.

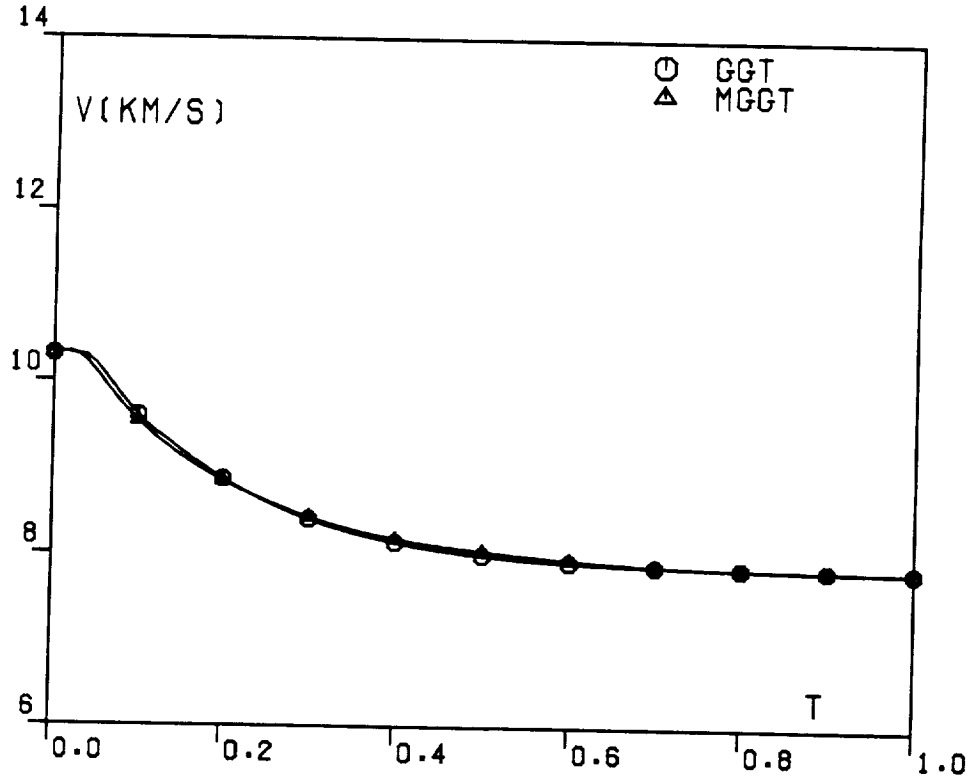

FIG. 7B. TRAJECTORY COMPARISON, CASE3.

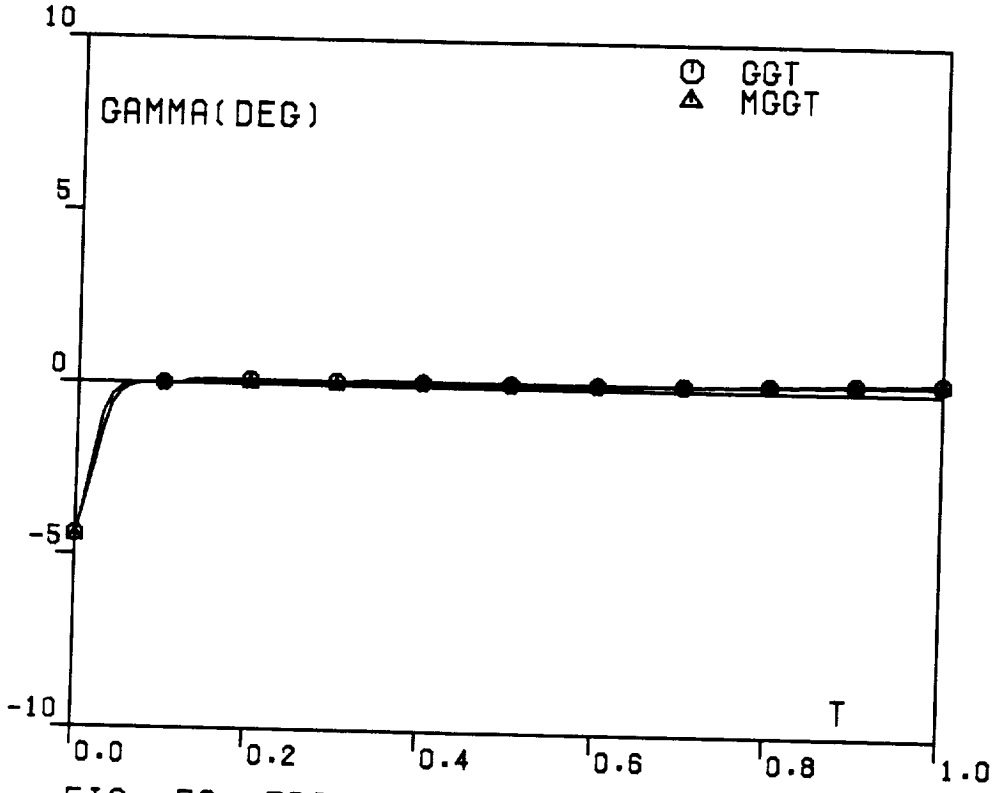

FIG. 7C. TRAJECTORY COMPARISON, CASE3.

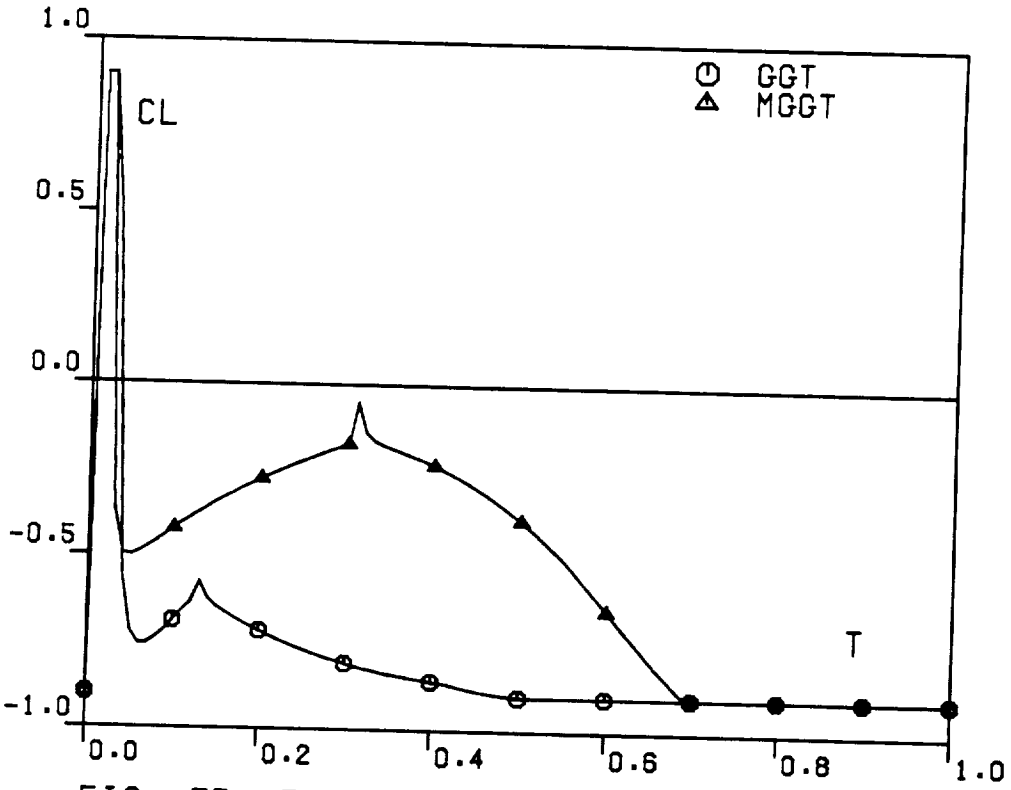

FIG. 7D. TRAJECTORY COMPARISON, CASE3.

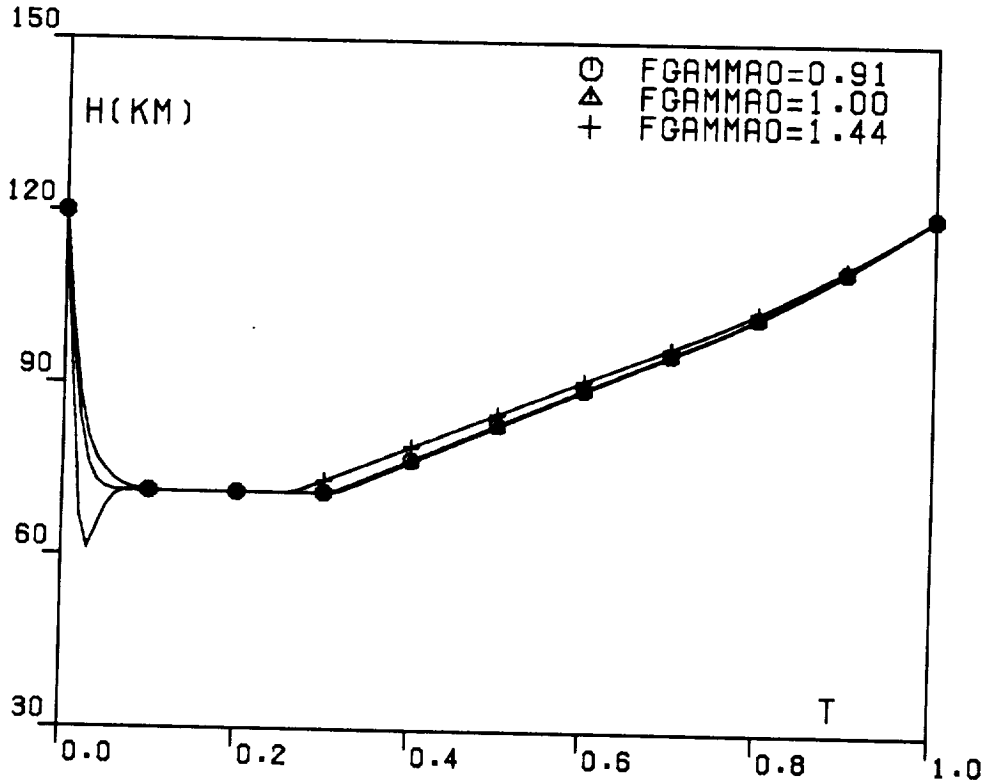

FIG. 8A. MODIFIED GUIDANCE TRAJECTORIES, ENTRY GAMMA CHANGE, CASE3.

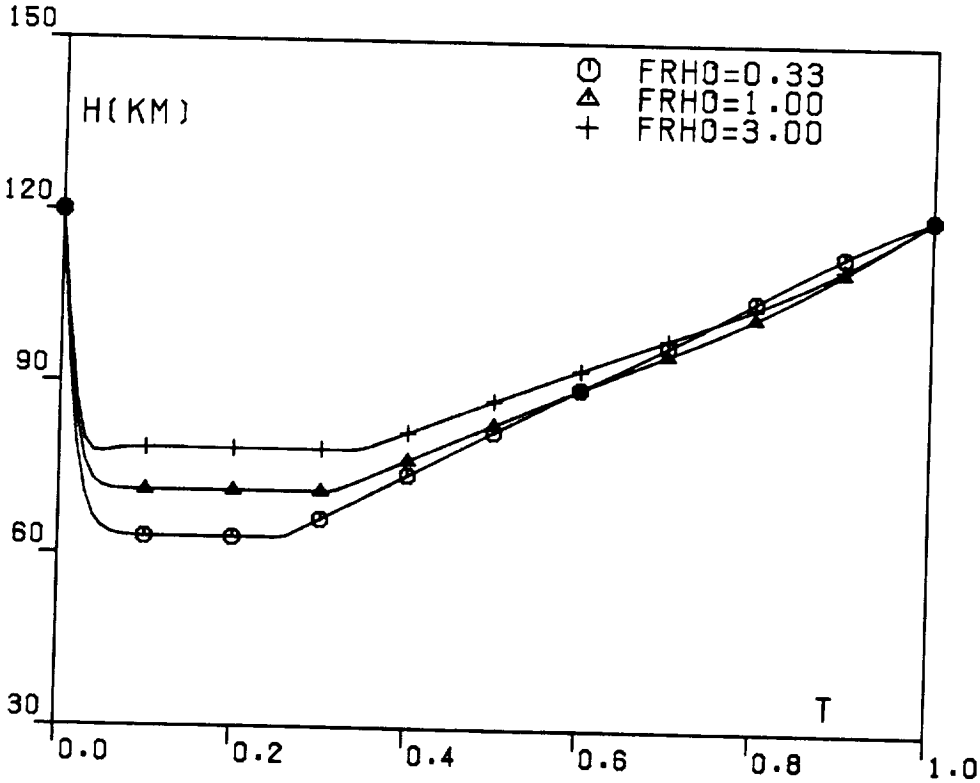

FIG. 8B. MODIFIED GUIDANCE TRAJECTORIES, DENSITY CHANGE, CASE3.

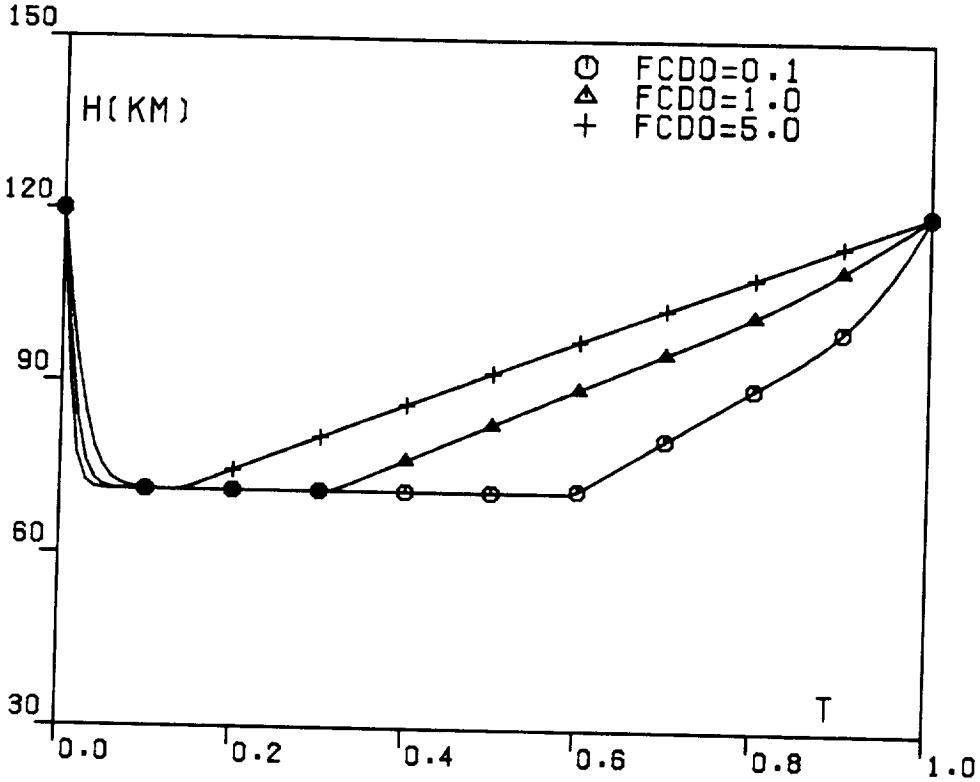

FIG. 8C. MODIFIED GUIDANCE TRAJECTORIES, ZERO-LIFT DRAG CHANGE, CASE3.

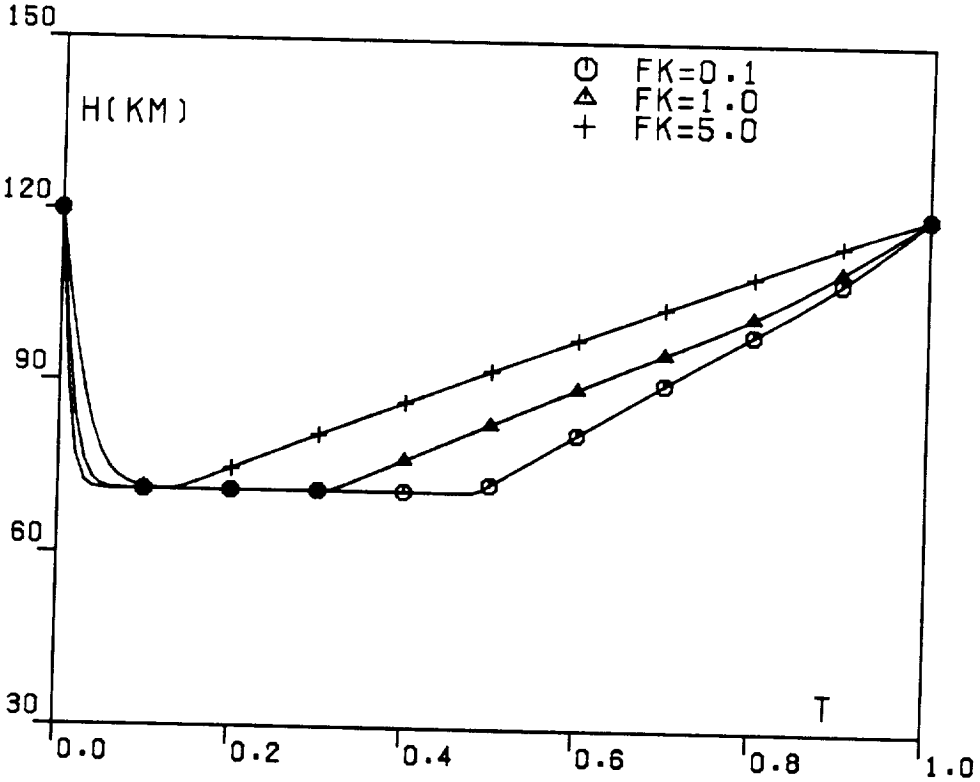

FIG. 8D. MODIFIED GUIDANCE TRAJECTORIES, INDUCED DRAG CHANGE, CASE3.

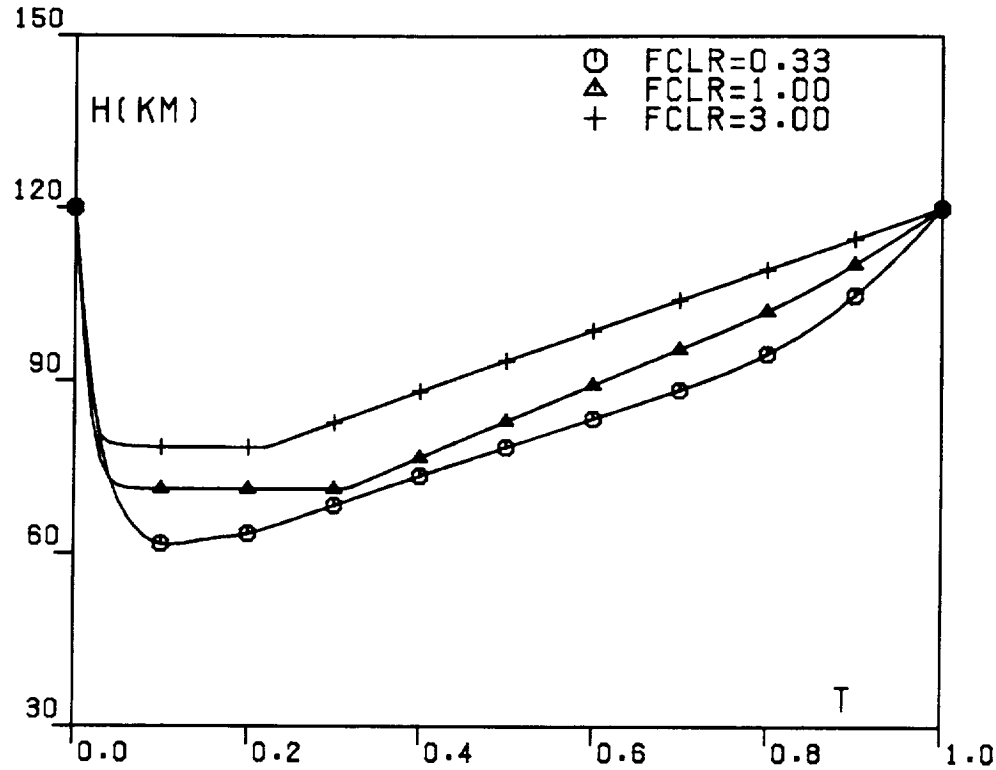

FIG. 8E. MODIFIED GUIDANCE TRAJECTORIES, LIFT RANGE CHANGE, CASE3.